Title

Enabling Multi-Zone Impedance Measurements for Higher Resolution Trans-Endothelial Electrical Resistance (TEER), and Single-Cell Viscoelastic Analysis.

Author

Falcon-Banchs, Roberto

Publication Date

2020

Peer reviewed|Thesis/dissertation

Enabling Multi-Zone Impedance Measurements for Higher Resolution Trans-Endothelial Electrical Resistance (TEER), and Single-Cell Viscoelastic Analysis.

By

Roberto Falcón-Banchs

A dissertation in partial satisfaction of the

requirements for the degree of

Joint Doctor of Philosophy

with the University of California, San Francisco

in

Bioengineering

in the

Graduate Division

of the

University of California, Berkeley

Committee in Charge:

Professor Lydia L. Sohn, Chair
Professor Tamara Alliston, UCSF
Professor Markita P. Landry

Fall 2020

Abstract

Enabling Multi-Zone Impedance Measurements for Higher Resolution Trans-Endothelial Electrical Resistance (TEER) and Single-Cell Viscoelastic Analysis.

By
Roberto Falcón-Banchs
Doctor of Philosophy in Bioengineering
University of California, Berkeley
Professor Lydia L. Sohn, Chair

The spatial and temporal resolution improvements of current and future biological assays are crucial elements in our advance toward single-cell assays, by which we dissect population-level averages to better understand disease progression and treatment. In this dissertation, spatial and temporal resolution improvements are demonstrated for two platforms by implementing a multi-zone measurement approach. For the first platform, we implement a multi-zone trans-endothelial electrical resistance (mz-TEER) continuous measurement within a microfluidic platform. This has enabled us to measure four distinct TEER zones within a single sample versus measuring one bulk TEER value. This work opens the door to questions of hetero- and homogeneity, and crosstalk between the cells on each of the respective zones. I will discuss how our results, using MCF-7GFP cell monolayers, showed that we are capable of monitoring these zones independently, and provide important future objectives for biologically relevant experiments, and improvements to the platform. Secondly, using the knowledge gained from developing mz-TEER, I then aimed to improve another impedance-based microfluidic platform developed in our lab previously, visco node-pore-sensing (viscoNPS) which is capable of measuring the viscoelastic properties of single cells at a single user-defined frequency. With an improvement similar to mz-TEER, we enhanced this platform by adding multi-zone measurement capabilities supported through the development of custom hardware and software, enabling each cell to be tested at up to four user defined frequencies.

To Lydia, thank you for being a source of inspiration, guidance and support.

To my fiancée Michelle and my family, thanks for the unconditional love.

Acknowledgements

First of all, I will like to thank my mentor, Prof. Lydia L. Sohn. You have been an amazing mentor during my years in your lab, and I cannot thank you enough. Together we have been through the ups and downs of the PhD: making sure you cheer me up when nothing was working, and celebrating with me when thigs worked out. I would have not accomplished this huge milestone in my life without you. I will also like to thank the other members of my dissertation committee: Prof. Tamara Alliston (UCSF), and Prof. Markita Landry (Berkeley). Your guidance and support through the process has been amazing.

I am deeply grateful of all the fellowships I received during my time as a PhD student, for the financial support and the great network of other fellows to which I have been connected. I want to thank the Berkeley Chancellors Fellowship, the National Science Foundation Graduate Student Research Fellowship, and the Siebel Scholars Program. Your support in my endeavor was a key part of completing my doctoral work.

I will like to thanks everyone in the Sohn Lab for both the scientific support and the friendships we have developed. Olivia Scheideler, Nahyun Cho, Junghyun Kim, Francois Rivest, Daniel Yang, Molly Kozminsky, Nate Liu, Brian Li, Kristen Corner, Thomas Carey, Rachel Rex, and Sean Kitayama. Our conversations have always been of key important in my work. I will also like to thanks Priya Vijaykumar for being such an amazing, talented, and dedicated undergraduate during our work together for the past two years.

Thank you to all the administrative staff that was somehow involved in my journey. Meltem Erol from the College of Engineering, for being such an amazing person and convincing me to come to Berkeley! Kristin Olson and Rocio Sanchez from the Bioengineering Department, for being great program advisors and helping with any of the issues that raised.

Lastly, I want to thank my family and friends for the support and love the have given me during this long process. My soon-to-be wife, Michelle, my parents Roberto Falcon and Patricia Banchs, and my sister, brother-in-law and niece (Natalia, Jose Carlos, and Emma).

What an amazing journey. To the friends I have gained during my PhD, now considered family, thank you. Anyone who I have missed in this section, Thank you.

Table of Contents

List of Figures

1 INTRODUCTION

Chapter Overview

This introduction summarizes the motivation for the research projects presented in this dissertation and provides a description of how the platforms that have been developed are based on similar resistance measurement principles. Furthermore, a brief description of the chapters that follow is provided.

1.1 Motivation

As beautiful and complex as they are, biological systems have challenged many scientists and engineers throughout history to develop new and creative approaches to improve our understanding of their complexity. Motivated by the heterogeneity of biology known to exist even within cell populations traditionally considered to be homogeneous, scientists and engineers are currently focused on achieving single-cell resolution for many "gold standard" biological assays, such as those that test for mechanical properties and those that seek to understand or uncover the protein profile of cells[1–7]. Single-cell resolution enables the detection of sub-populations that were not previously known and gives insight into the importance of the heterogeneity in a population. This has proved important in the detection, monitoring, and treatment of diseases such as cancer[8–11].

Cancer is the second leading cause of death in the United States[9]. Researchers have continued to focus their efforts in understanding how cancer develops and what causes its progression and metastases to help in the development of more effective therapies[5,12,13]. During metastasis, cancer cells from the primary tumor, which are more mechanically compliant than non-cancerous cells, migrate through the extracellular matrix (ECM) and endothelium in a process called intravasation[14,15]. After crossing the endothelium, cells that reach the blood stream are referred to as circulating tumor cells (CTCs). CTCs traverse the vasculature and exit the blood stream through a process called extravasation. During this process, CTCs adhere to the endothelium using selectins (P- and E- selectins), ligands, and surface integrins (ICAM- 1 and 2)[14,16]. They then cross through the endothelium's cell-cell junctions, and establish a secondary tumor[16].

As explained previously, the endothelium, a layer of endothelial cells lining the blood vessels in the human body, plays an important role during the metastatic process[17–19]. Because of the complexity of this microenvironment, the development of *in-vitro* models serves as tools to study how the endothelium regulate cell migration, for example, during metastasis[20,21]. One of these tools, the Transwell Assay (TA), is regarded as the "gold standard" for cell migration and endothelium barrier function studies[19,22,23]. In a Transwell Assay, endothelial cells are cultured on a porous membrane insert, allowing access to both the top (apical chamber) and bottom (basal chamber) sides of the monolayer. This experimental setup is commonly used to evaluate the metastatic potential of cells by adding them to the apical chamber and evaluating how many cells cross the endothelial cell monolayer within a fixed amount of time[16,21].

Transwell Assays also allow scientists to study the barrier function of the endothelial monolayer. To do this, a trans-endothelial electrical resistance (TEER) measurement is performed, which measures the average electrical resistance across a monolayer. The applied electrical current crosses the monolayer through cell-cell junctions, thus serving as a quantitative assay that evaluates the overall monolayer barrier function[24]. In contrast to end-point measurements that assess cell-cell junctions, such as immunofluorescence, TEER measurements can be repeated without negative effects to the monolayer, making it a widely used technique[22,24–27].

Although single-cell resolution in TEER is not possible since cell-cell junctions are required, this dissertation focuses on the implementation of multi-zone, real-time electrical resistance measurements within microfluidic platforms, with the overall goal of increasing the spatial and temporal resolution of TEER measurements. I will show how the multi-zone approach inside a microfluidic channel, allows the platform to reduce the number of cell-cell junctions being measured, thus reducing the effects of bulk averages. After describing the development of a microfluidic-based multi-zone platform to measure TEER (mz-TEER), we will discuss how the knowledge from this project was applied to another microfluidic platform to improve resolution. As previously mentioned, TEER is the gold standard measurement for monolayer barrier function. Measuring the resistance across a monolayer of cells provides information about cell-to-cell junctions and their function. In contrast to the single bulk resistance value obtained with the TEER measurement, our platform measures TEER values from four distinct zones along a single monolayer. This technology enables a more accurate assessment of the homo- or heterogeneity of endothelial cell monolayers, which would lead better *in-vitro* endothelium models advancing fields that relay on TEER (e.g. drug delivery). In addition, mz-TEER enables studies of zone-specific perturbations, in which some zones of the monolayer are exposed to specific biochemical cues and the control zones can be monitored to understand crosstalk along the sample. This intra-monolayer experimentation had not been previously possible[22,28].

Developing mz-TEER required custom electronics and software that could measure electrical resistance in various zones within the device. Applying this knowledge to a platform developed in the Sohn Lab, we advanced single cell viscoelastic measurements using microfluidics[29]. This proof-of-concept setup increases the platform's capability to measure the electrical resistance from one to four distinct zones along a microfluidic channel. When coupled with single-cell viscoelastic measurements, this results in the interrogation of single cell viscoelastic properties at four frequencies, instead of one, allowing mathematical material modeling [29]. As shown in Figure 1-1, techniques used to create multi-zone impedance measurements used in mz-TEER were used to develop a proof-on-concept setup using visco-NPS. With this new multi-zone visco-NPS (mz-viscoNPS), multiple frequencies can be applied to a single cell for measurement, enabling the fit of material models to each cell, instead of population-level averages. Figure 1-2 shows images of both platform after assembly.

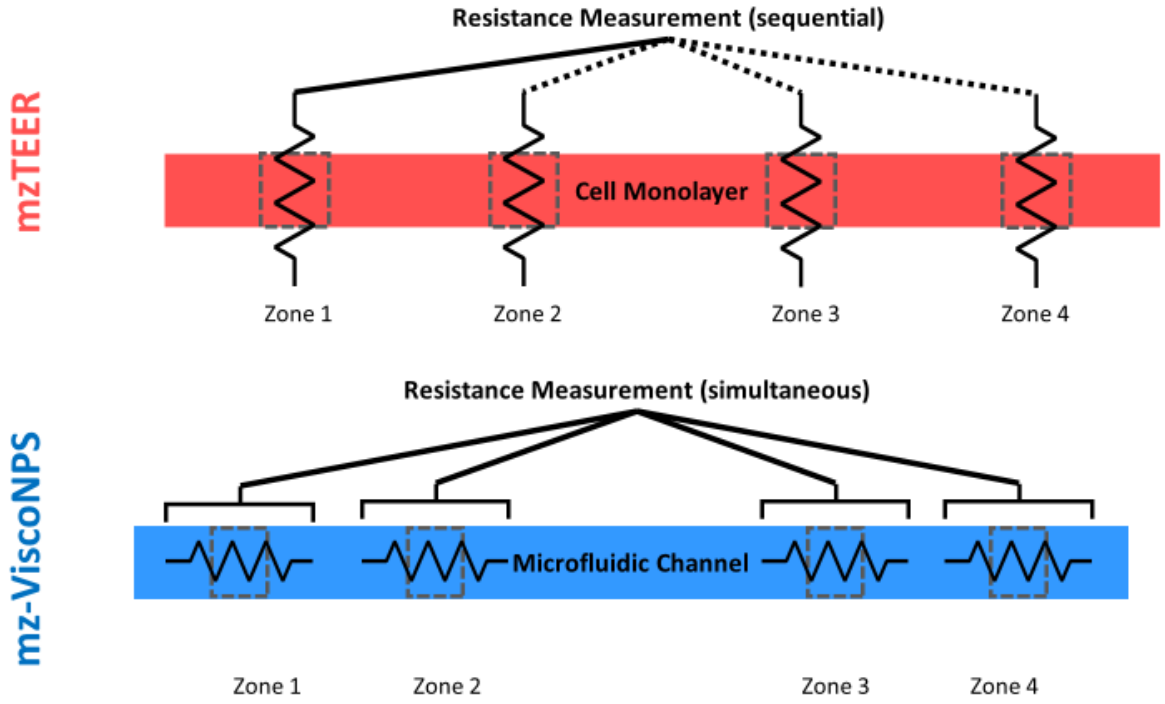

Figure 1-1 Measurement setup for mz-TEER and mz-viscoNPS. Top: During multi-zone TEER, we sequentially measure resistance across the monolayer at each of the four measurement zones. Bottom: For mz-viscoNPS, the resistance is measured simultaneously in all four contraction channels in which the viscoelastic properties of cells are measured.

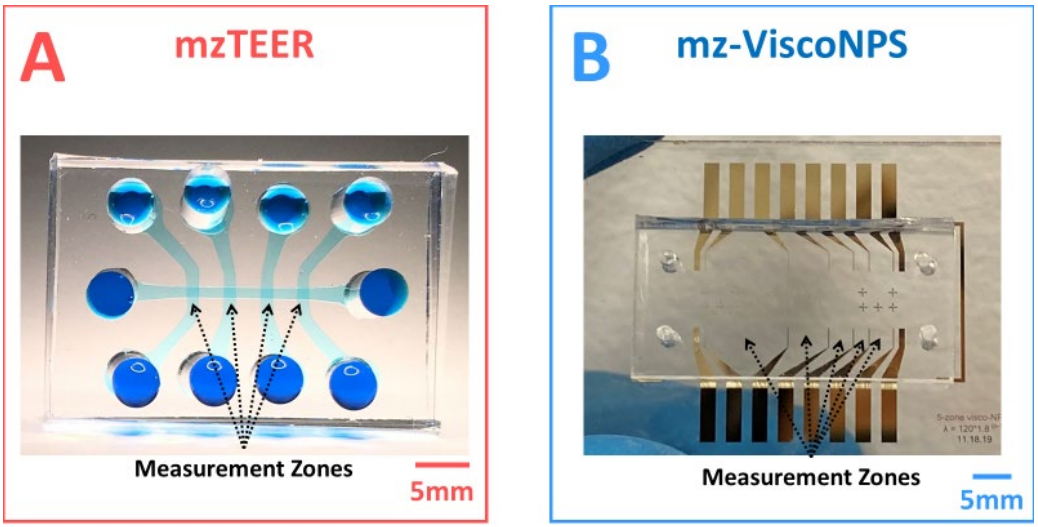

Figure 1-2 Finalized microfluidic platforms. A, Top view of mz-TEER platform with arrows indicating the measurement zones. Blue food dye used to increase contrast. B, Top view of a proof-of-concept multi-zone viscoNPS device. Arrows show space between electrodes where the contraction channels are located.

1.2 Organization of the Dissertation

This dissertation begins with an introduction to the important engineering principles upon which the two platforms are based. Thereafter, the dissertation delves into the development of the mz-TEER microfluidic platform and then on the mz-viscoNPS. Finally, this dissertation concludes with important findings and recommendations for future research.

- **CHAPTER 1: INTRODUCTION**
  This chapter summarized the motivation for the research, discussed important similarities between the projects to be presented, and the organization of the chapters in this dissertation.

- **CHAPTER 2: ENGINEERING PRINCIPLES**
  This chapter discusses the engineering principles and design considerations used for the development of mz-TEER and mz-viscoNPS.

- **CHAPTER 3: DEVELOPMENT OF A MICROFLUIDIC-BASED MULTI-ZONE TRANS-ENDOTHELIAL ELECTRICAL RESISTANCE**
  This chapter presents the development of the mz-TEER platform. Furthermore, it describes fabrication techniques employed, computational modelling, and the protocols created for cell culture and device sterilization.

- **CHAPTER 4: RESULTS AND VALIDATION FOR MICROFLUIDIC-BASED MULTI-ZONE TRANS-ENDOTHELIAL ELECTRICAL RESISTANCE**
  This chapter describes the validation and experimental results for the mz-TEER platform introduced in Chapter 3.

- **CHAPTER 5: MULTI-ZONE IMPEDANCE MEASUREMENTS FOR VISCO-NODE-PORE SENSING**
  This chapter delves into the development of a proof-of-concept setup that employs a multi-zone approach, similar to mz-TEER, aiming to advance single-cell viscoelastic measurements.

- **CHAPTER 6: CONCLUSIONS AND FUTURE RESEARCH**
  This chapter summarizes the results of the technologies presented in this dissertation and provide overall conclusions, and future work for design improvements and assay development.

2 ENGINEERING PRINCIPLES

Chapter Overview

This chapter highlights the key engineering principles used in the research discussed in this dissertation. This chapter is divided into three key sections. In the first section, I will discuss the impedance measuring techniques that is used in both mz-TEER and mz-ViscoNPS. In the second section, I will describe the engineering principles used by each of the platforms. In the third section, I will summarize the key elements discussed.

2.1 Principles of Four-Probe Impedance Sensing

As discussed before, this dissertation presents the development of two separate platforms, that although having different applications, have the same readout: electrical impedance. In this section, I will discuss the principles of electrical impedance, how it can be measured, and the reasoning for choosing the methods we use. Details on how impedance sensing is applied to each of the platforms will be discussed in the next two sections.

Electrical impedance is the measure of a component's opposition to the flow of current when an electric potential is applied across it[30]. This model is described by Ohm's Law,

$$\boldsymbol{V = IR} \tag{1}$$

where V is the electric potential expressed in volts (V), I is the current expressed in amps (A), and R is the resistance expressed in Ohms (Ω). The most commonly used technique to measure resistance is a two-probe measurement[31,32]. This technique employs a voltage divider, which uses a known reference resistor to calculate the voltage drop across an unknown resistor[32].

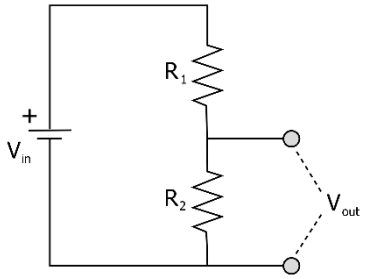

Figure 2-1 Electronic schematic of a voltage divider circuit. This circuit is used to calculated an unknown resistance (R_2) by applying a known voltage (V_{in}), having a resistor (R_1) with known value in series, and measuring the voltage across the unknown resistor (V_{out}). See equation 2 to calculate R_2.

Using Kirchhoff's Law, we find that:

$$R_2 = \frac{V_{in} - V_{out}}{V_{out}} R_1 \quad (2)$$

A two-probe measurement excels when precision is not required. However, when applied in microfluidics systems, this measurement is prone to error because of the formation of an electric double layer (EDL) that surrounds the measurement electrodes. Specifically, when electrodes are exposed to an electrolyte (cell media), and EDL of thickness equal to the Debye length, λ_d, forms:

$$\lambda_d = \sqrt{\frac{\varepsilon_0 \varepsilon_r kT}{2N_A e^2 I}} \quad (3)$$

where, I is the ionic strength of the electrolyte, ε_0 is the permittivity of free space, ε_r is the dielectric constant of the electrolyte, k is the Boltzmann's constant, T is temperature, N_A is Avogadro's Number, and e is the elementary charge. An EDL forms because positive-ions in the are attracted to the negatively biased electrode, and negative-ions are attracted to the positively biased electrode. This leads to an additional resistance measured (see Figure 2-2)[33]. To remove this added resistance, a four-probe measurement can be performed. In such a measurement, the current and voltage leads are separated and the resistance caused by the EDL is not measured[32,34].

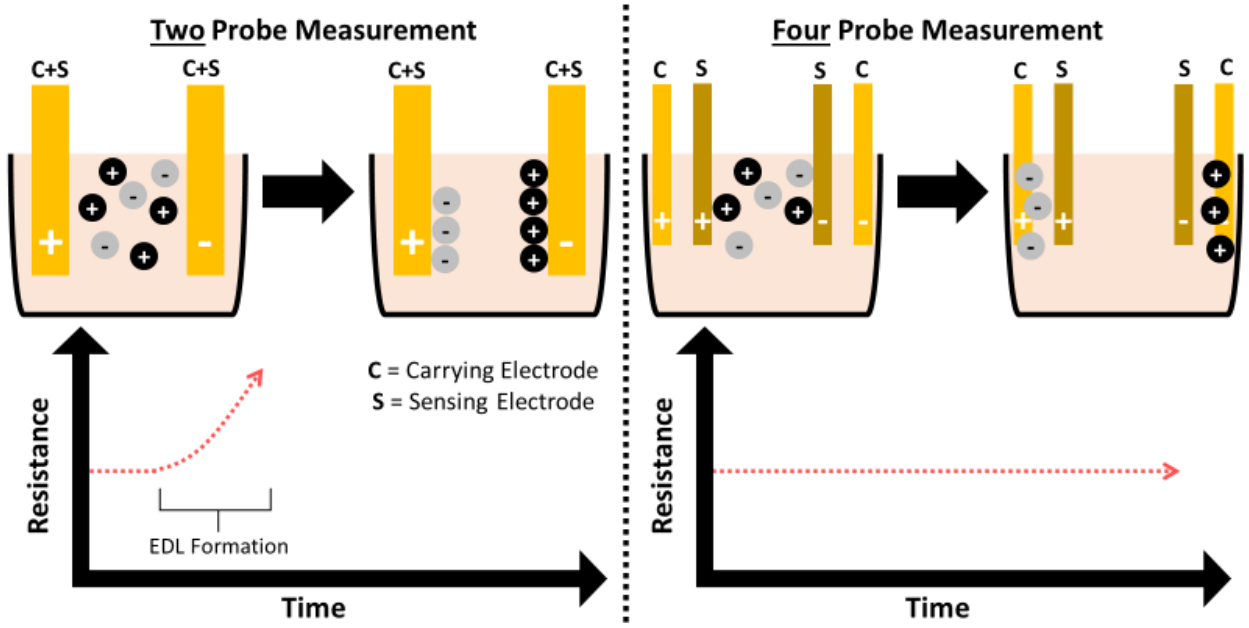

Figure 2-2 Comparison between two-probe and four-probe resistance measurements. Left: A two-probe setup with electrodes in contact with an electrolyte (e.g. cell media). The formation of an electrical double layer (EDL) leads to an increase in measured resistance due to the EDL acting as an insulator. Right: A four-probe measurement. In contrast with a two-probe setup, the EDL forms on the carrying electrodes. The sensing electrodes are not affected, thus providing a stable, accurate resistance measurement.

2.2 Trans-Endothelial Electrical Resistance Measurements

Transwell-Assays (TA) are the gold standard for *in-vitro* endothelium models[19]. In a TA, endothelial cells are grown into a monolayer on top of a porous membrane that sits on a well-plate insert (Fig. 2-3)[19,21]. To characterize and validate the monolayer growth, a trans-endothelial electrical resistance (TEER) measurement is performed. Such a measurement provides information on whether the monolayer is completely confluent and whether cell-cell junctions have formed, at which point the TA can be used for specific biological experiments.

In more detail, TEER is a four-probe measurement that is performed across the monolayer, from the apical to the basal side. By measuring the current that flows across the cell-cell junctions from the apical to basal side, one can determine how tight or loose these junctions are in the monolayer. Typically, however, TEER measurements in TA are mainly used to detect when the barrier function is reached (100% confluency)[19,35,36]. Because TA inserts all vary in size, the resistance values measured are multiplied by the membrane area (R*A, where R is resistance and A is the area of the TA insert) in order to obtain a TEER value (units: $\Omega \cdot cm^2$).

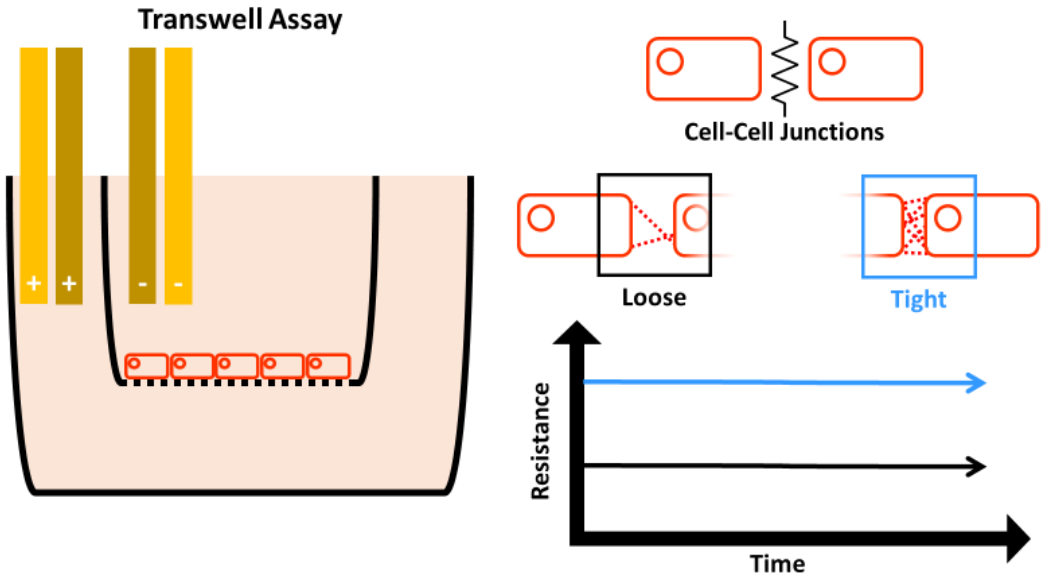

Figure 2-3 Transwell Assay (TA) schematic with the corresponding trans-endothelial electrical resistance (TEER) measurement. Left: The TA uses an insert with a porous membrane on top of which endothelial cell monolayers are cultured; electrodes are inserted to take a four-probe measurement of resistance across the cell layer and porous membrane. Right: an illustration of how TEER is used as a quantitative proxy assay to study cell-cell junctions.

For commonly used human umbilical vein endothelial cells (HUVEC) and human cardiac microvascular endothelial cells (HCMEC), expected TEER values when barrier function is achieved is $80 \pm 10\ \Omega \cdot cm^2$ [24,37]. Researchers have used shear stress and chemokines (e.g. TNF-alpha) to stimulate the loosening or tightening of cell-cell junctions. Specifically, when HUVEC cells were exposed to shear stress (10 dyne/cm^2) in a microfluidic TA, TEER values decreased by 18% as compared to when compared to when there was no shear stress[27]. As another example,

when HUVEC monolayers are exposed to TNF-alpha, they loosen their cell-cell junctions and this is leads to a 22% decrease in TEER. The effect of shear stress and TNF-alpha is synergistic, and when combined, TEER is reduced by 35% [38].

The importance of a TEER measurement in TA cannot be understated. Drug delivery experiments rely heavily on TAs to provide a quantitative *in vitro* model of how a certain drug compounds cross the endothelial cell monolayer[27,39,40]. Testing drug absorption, the necessary carriers to increase the efficiency of that absorption, and drug concentration can be accomplished with a TA.

TEER measurements performed in TAs provide information on the bulk properties of an endothelial monolayer. Current TA platforms, even those that integrate microfluidics, only provide bulk information of the endothelial monolayer. They assume that the cell-cell junctions are homogeneous across the monolayer. To improve the spatial and temporal resolution of TEER measurements, we have developed multi-zone TEER (mz-TEER), shown in Figure 2-4. mz-TEER is a microfluidic platform that allows apical and basal access to specific areas of a monolayer. We enable spatial resolution by monitoring TEER in four separate zones of the monolayer, resulting in four distinct TEER values within a sample, a first for a TEER based platform. mz-TEER also measures each zone every 15 seconds, representing an improvement in obtaining temporal information when compared to previously published microfluidic platforms that measured at the minute time-scale[41,42]. Overall, mz-TEER's multi-zone capability can advance our understanding of the barrier function heterogeneity within an endothelial monolayer. In Chapters 3 and 4, I go into greater details of the design and measurement of mz-TEER.

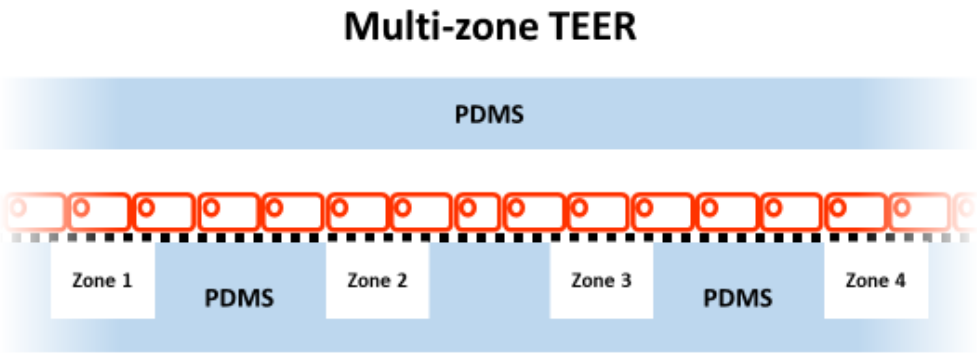

Figure 2-4 mzTEER schematic.

2.3 Principles of Visco Node-Pore-Sensing

Visco Node-Pore-Sensing (ViscoNPS) employs the principles of Resistive-Pulse Sensing (RPS) to measure the viscoelastic properties of cells[29,33,43,44]. In this section, I will first discuss the principles of RPS and how these have been leveraged by the Sohn Lab to develop platforms to measure various properties of cells, including their viscoelastic properties[29].

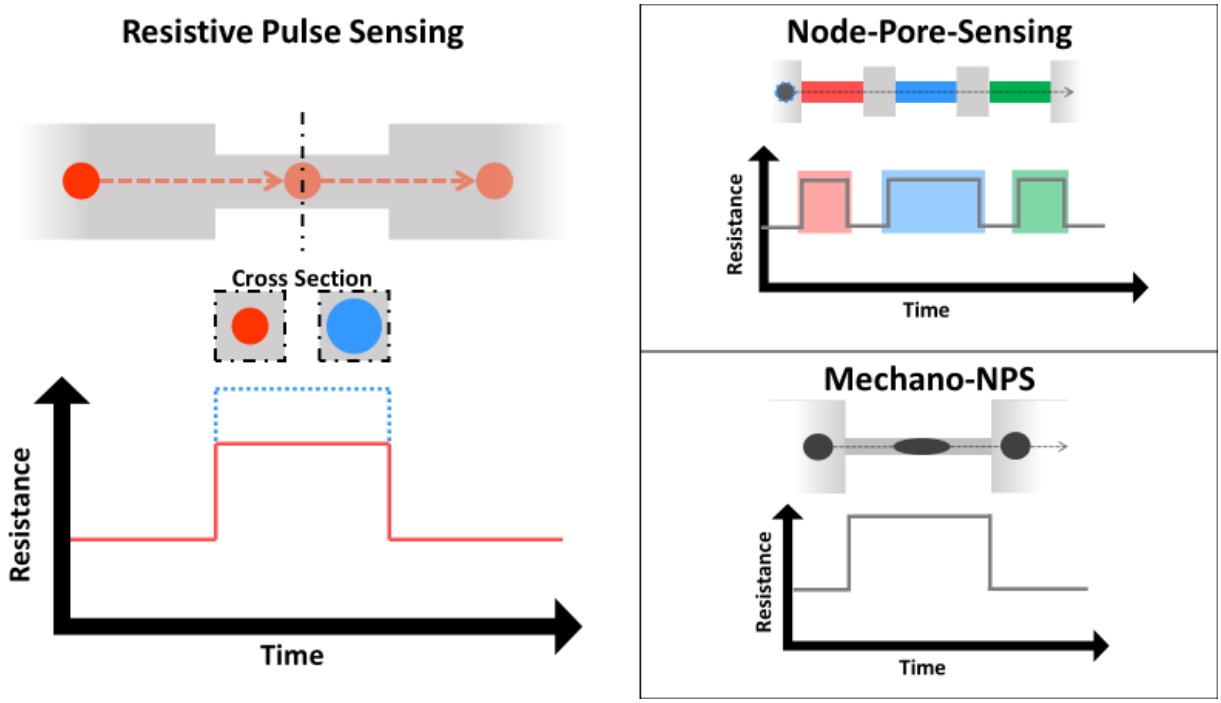

Figure 2-5 Descriptions and illustrations of Resistive Pulse Sensing (RPS), Node-Pore-Sensing (NPS), and Mechano-NPS. Left: RPS works by measuring the electrical resistance of a pore filled with a conductive fluid. When a non-conductive particle passes though the pore it displaces conductive fluid and temporarily increases the pore resistance, thus producing a resistance pulse. The pulse magnitude is correlated with particle size as illustrated by the red and blue particles and their respective signals. Right, top: In NPS, consecutive pores are patterned with antibodies of interest that interact with cell surface markers, slowing down cells as they transit regions patterned with antibodies for which they have receptors. A cell's transit times through each pore are compared to determine which cell surface markers are expressed. In this schematic, the cell is positive for the blue surface marker, resulting in a longer blue pulse. Right, bottom: Similarly, mechano-NPS uses transit time through a contraction channel, generally inversely correlated with cell stiffness, to mechanically phenotype single cells.

RPS involves performing a four-probe measurement across a microfluidic channel. When a cell, transits the channel, a resistive pulse is measured. This pulse is caused by the cell partially blocking the flow of current. The pulse magnitude corresponds to the size of the cell and the pulse duration corresponds to the cell's transit time across the channel. When nodes (i.e. widen areas) are inserted in the channel and consequently segment the channel, the resistive pulse of a cell is modulated. This modulation is due to the fact that the cell blocks different proportions of current

flow in a node vs the segment between the nodes. With "node-pore sensing" (NPS), one can use the modulated resistive pulse to determine where the cell is at any given time in the channel. When one of the segments between the channel is much narrower than the diameter of a cell, a cell must squeeze through in order to transit the entire NPS channel. As such, one can determine the mechanical properties of the cell, including the cell size, the resistance to deformation, and recovery from transverse deformation. "mechano-NPS" has proved to be a rich platform and has been used to differentiate malignant (MCF-7) and non-malignant (MCF-10A) breast epithelial cells and to identify chronological age differences in primary human mammary epithelial cells[44].

Recently, mechano-NPS was advanced even further—this time by including a sinusoidal "contraction channel". As it transits the channel, it undergoes periodic deformation within that sinusoidal contraction channel. The resistive pulse measured is sinusoidal and one can extract viscoelastic properties (G' and G" corresponding to elasticity and viscosity, respectively). "visco-NPS" has been used to determine the contributions of different cellular components (e.g. cytoskeleton, nucleus) that contribute to the viscoelastic properties of MCF-7 and MCF-10A cells. This platform successfully measured the viscoelastic properties of malignant and non-malignant cells and enabled the use of a Kelvin-Voight material model to better elucidate differences between populations[29]**.** While visco-NPS presents a high-throughput method of measuring the viscoelastic properties of cells (vs. the gold standard of atomic force microscopy or micropipette aspiration, each of which analyze 1-2 cells/hr), this method can only measure the bulk properties of cells. Specifically, visco-NPS can only measure a single cell at one particular frequency. In Chapter 5, I will discuss a proof-of-concept platform, multi-zone visco-NPS, which enables measuring the viscoelastic properties of single cells at four different frequencies. Multi-zone visco-NPS takes advantage of the hardware, software, and knowledge gained from mz-TEER's development.

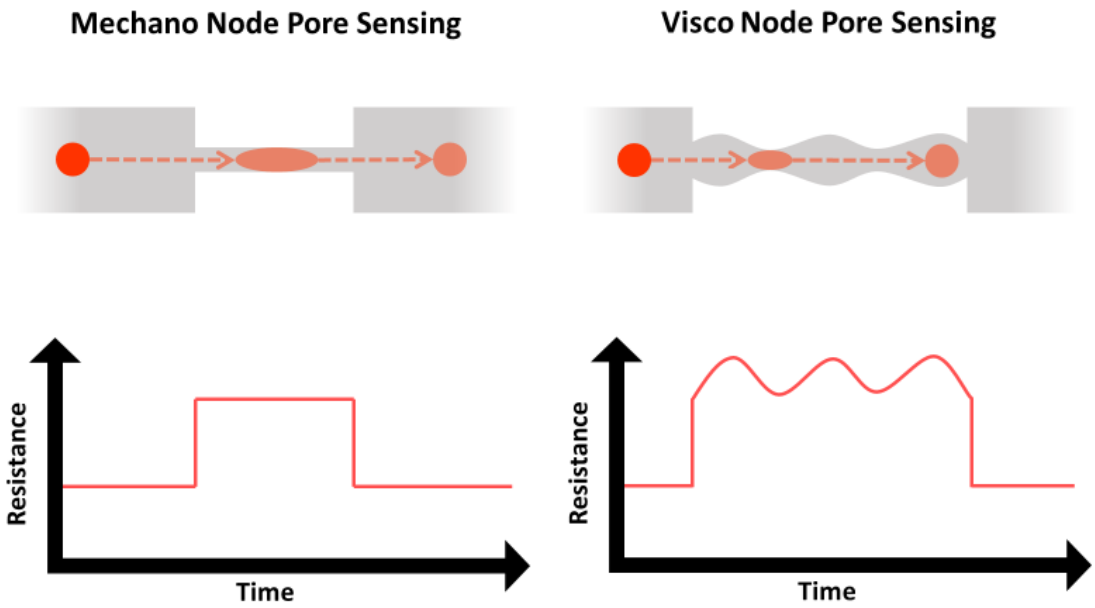

Figure 2-6 Difference in resistance pulse from mechano-NPS and viscoNPS. Left: mechano-NPS generates a constant pulse that starts when the cell enters the contraction channel and returns to baseline when the cell exits. For viscoNPS, shown on the right, the pulse has a sinusoidal shape corresponding to the sinusoidal contraction channel.

2.4 Conclusion

As discussed in the previous sections, the technologies that are detailed in the following chapters are based on four-probe resistance measurements. By using the engineering principles discussed and integrating a multi zone approach into the development of our platforms, we aim to increase the assays spatial and temporal resolution. For mz-TEER, measuring four distinct zones, instead of one bulk average, will allow our platform to answer questions regarding the heterogeneity of cell-cell junctions within a monolayer. These results will guide us to better understand the complex endothelium microenvironment. As with the mz-viscoNPS platform, our goal is to use this proof-of-concept to inform the development of the next generation viscoNPS to improve our current single-cell viscoelastic capabilities, thus eliminating the use of averaged populations. In the following chapter I will delve into the design, fabrication, and validation of the multi-zone TEER device.

3 DEVELOPMENT OF A MICROFLUIDIC-BASED MULTI-ZONE TRANS-ENDOTHELIAL ELECTRICAL RESISTANCE

Chapter Overview

In this chapter, I will discuss the design and fabrication of a novel microfluidic-based multi-zone TEER sensing platform. This new device, is capable of measuring TEER along specific zones within the same sample, thus improving the resolution of current technologies which provide only one bulk average value. Furthermore, the development of the custom hardware and software will be discussed. I will discuss possible areas of optimization regarding the platform's design and operation. The following chapter will include the validation, results, and modelling of this platform.

3.1 Introduction

Given the complexity of the endothelium microenvironment *in-vivo*, the development of *in-vitro* models has been of great importance. Much of the progress in developing *in-vitro* models has been led by drug delivery research[27,39,45,46]. Understanding how drug candidates affect and cross the endothelium when absorbed by the body, is a crucial step in the drug approval process. The current gold standard for *in-vitro* endothelium models is a Transwell Assay (TA)[19,47] . As detailed on Chapter 2.2, this assay involves the formation of an endothelial cell monolayer on top of a porous membrane. This membrane is suspended in a well plate insert that allows access to both the apical(top) and basal(bottom) sides of the monolayer, and in turn, enables trans-endothelial electrical resistance (TEER) measurements as a means to characterize the monolayer[19,22]. As detailed in this chapter, access to both sides of the monolayer is a key design feature that I have integrated into my microfluidic platform.

Current commercially available technologies (e.g. EVOM2, World Precision Instruments) that enable TEER measurements employ two different electrode pairs for a four-terminal measurement: one pair is inserted in the apical chamber, and the other in the basal chamber[28]. Although performing TEER in this manner has been successfully employed for years, it has some fundamental limitations. First, it only provides one bulk average resistance value per monolayer. This is problematic if the monolayer has a small imperfection in the monolayer confluency, as this will act as an electrical sink and current will flow through this imperfection instead of through cell-cell junctions[24,27,28]. Second, the electrodes do not provide a homogeneous potential across the sample, which leads to measurement bias and error[28]. Third, the user often manually holds the electrodes in place for measurement, requiring the sample to be taken out of the incubator and increasing the chance of contamination due to constant user-sample interaction. Fourth, temporal resolution is limited since each measurement is performed individually[21,24,36,48].

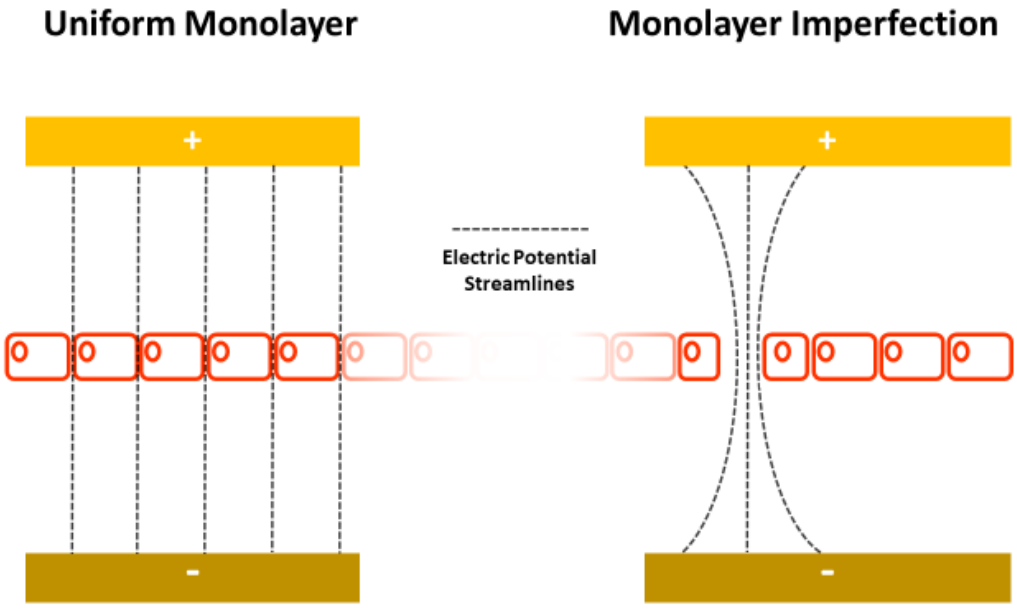

Figure 3-1 Effects of monolayer imperfections on TEER measurements. Left: On a uniform monolayer, cells are equally distributed and fully confluent, resulting in accurate TEER measurements. Right: An imperfection is present, due to cell death or incomplete confluency, resulting in non-uniform current flow and thus compromising the measurement.

Improvements to TEER measurements have involved smaller TA inserts (smaller monolayer area), and the use of measurement correction factors[28]. Yet, these improvements still do not provide sufficient spatiotemporal resolution necessary for transmigration events, where malignant cells cross the monolayer. Recently, microfluidics has been integrated with TEER measurements[22,24,26]. Although microfluidics offers the potential to create vessel-like microenvironments (organ-on-a-chip), and the addition of shear stress (fluid flow), TEER measurements still suffer from the same aforementioned limitations: only bulk values of the monolayer are obtained and manual measurements are still performed[27,36,38,39].

Here, we present a microfluidic platform that enables TEER measurements with: 1) high temporal resolution, as measurements are taken ever thirty seconds automatically, and 2) spatial resolution by measuring up to four distinct areas within the same monolayer. Our platform consists of a two-layer polydimethylsiloxane (PDMS) with a porous membrane in the middle. This construction, as shown on Figure 3-2, mimics a Transwell Assay (TA), by enabling access to the apical and basal sides of the monolayer via top and bottom chambers. Through microfluidic fabrication, we divide the basal chamber into specific measurement zones, as shown in Figure 3-2, which enable mz-TEER. Such an approach enables such novel zone-specific experiments as the spatiotemporal response of a monolayer to a specific cue (i.e. drug). In this chapter, we will detail the design and fabrication process of the mz-TEER platform.

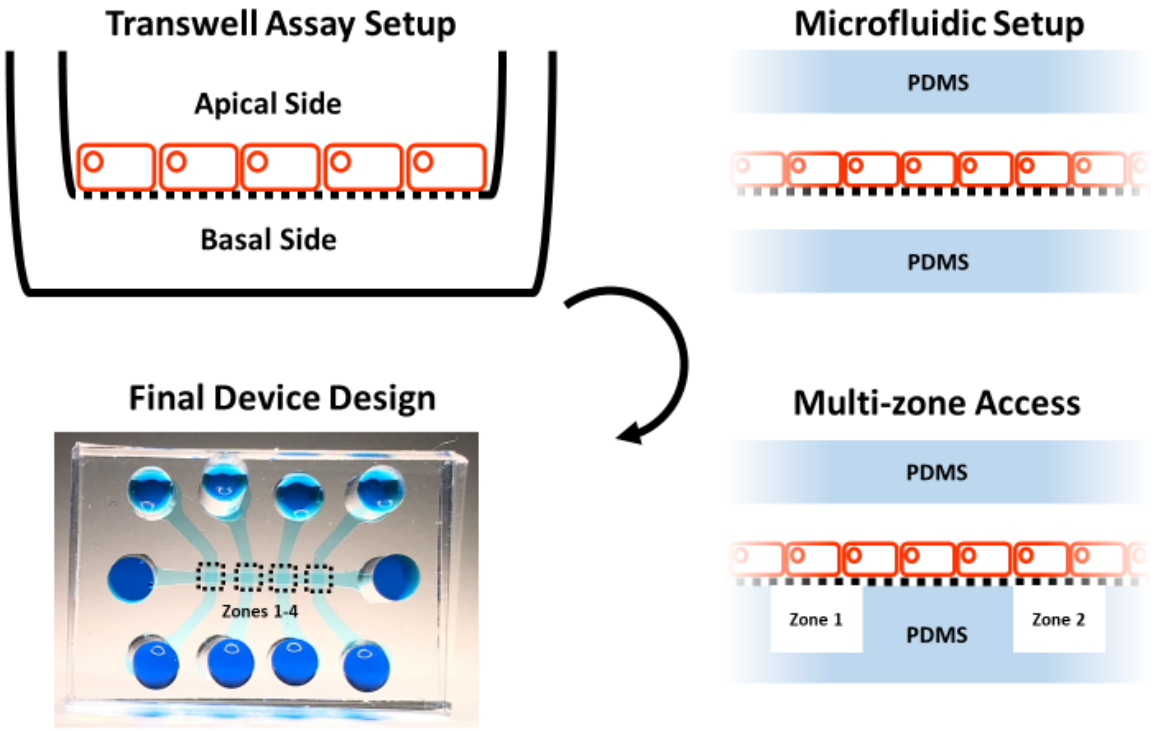

Figure 3-2 mz-TEER platform development process. As with the Transwell Assay (TA), a key design consideration is the access to the apical and basal side of the monolayer need to measure TEER. A traditional TA setup uses a well plate with custom inserts that have a porous membrane that separates the apical a basal chamber. When integrated into a microfluidic setup, the same access is obtained by leveraging a two-layer PDMS device that house a porous membrane in-between.

3.2 Platform Design and Fabrication

This section includes key aspects of the design process and selection, the development of fabrication protocols, details on the computational model used for validation, and the final device including the custom hardware and software that complete the platform.

3.2.1 Device Design

Through microfluidic channels, our platform provides access to both the apical and basal side of a monolayer. TEER measurements can thus be performed. As well, a user can easily expose either side of the monolayer to specific chemical cues to thus study its spatiotemporal reaction. To create the monolayer, cells are cultured on top of a 10 µm-thick polyester membrane consisting of 2µm-large pores (Sterlitech Corp., USA).

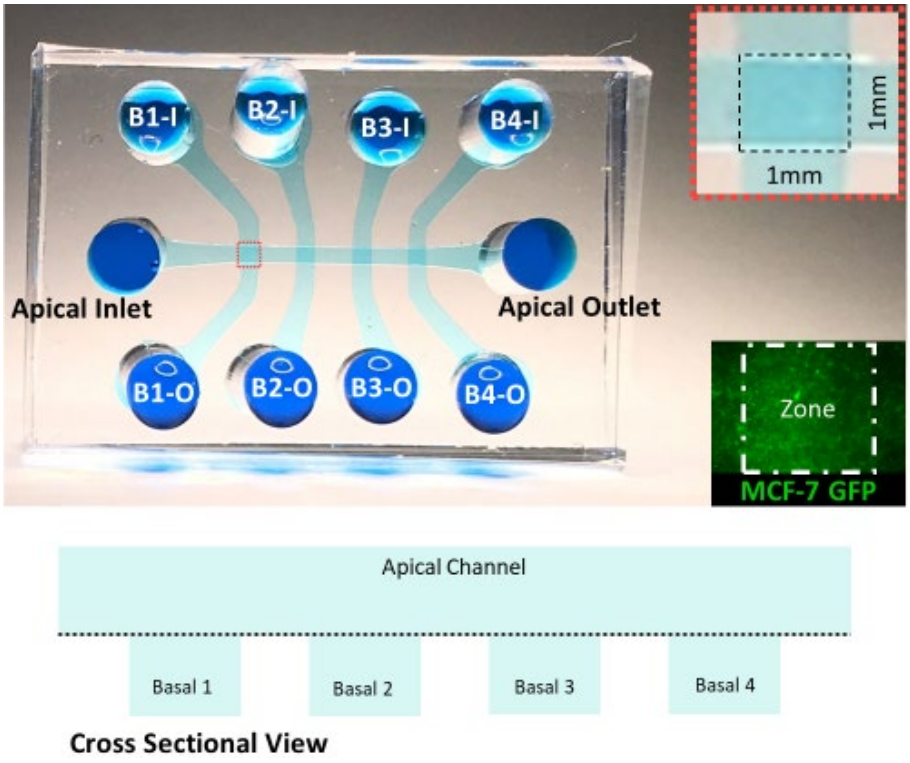

Figure 3-3 Finalized mz-TEER device. The top view (top) shows the function of each inlet and outlet. The apical channel is a single straight channel in which the cells are loaded and the monolayer forms. As shown in the cross-sectional view, the basal channels are orthogonal to the apical channel, forming four measurement zones where the channels intersect. The top inset shows a magnified, dimensioned view of a single zone. The bottom inset is a micrograph of an MCF-7GFP monolayer; dashed line indicates the zone's perimeter.

Although our two-layer design is similar to previously published devices for TEER measurements, our added zone-specific access through multiple basal fluidic channels is entirely unique and advantageous, as described above[22,24,26,27]. Figure 3-3 shows a completed device with four 1mm x 1mm (L x W) zones and a fifth zone (the apical channel itself), which monitors cell media

conditions. All measurements are performed using a custom electrode interface that was designed and fabricated to fit with our PDMS device. Below we provide the details of the device design and fabrication, and the development of the custom hardware and software that enable mz-TEER measurements.

3.2.2 Microfluidic Device Fabrication

The mz-TEER platform is fabricated using soft-lithography, which involves casting a polydimethylsiloxane (PDMS) mold from a lithographically defined negative master. In more detail, two lithographic masks, which define the top and bottom PDMS layers, were designed via AUTOCAD.

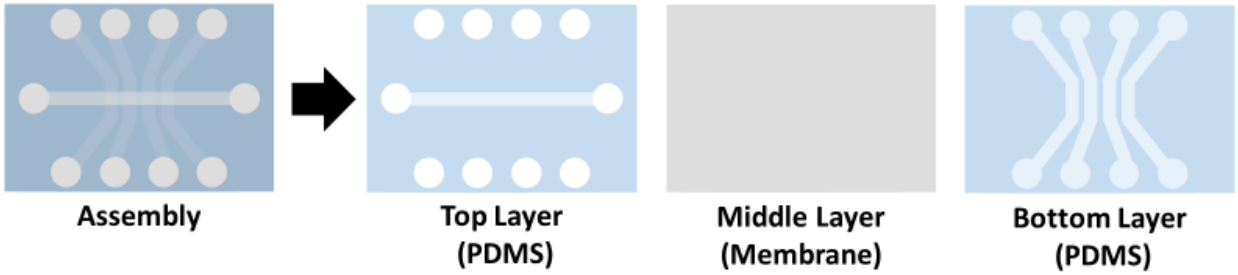

Figure 3-4 Exploded view of multi-zone TEER device. The top layer, made from PDMS, houses the apical channel and the inlets/outlets for all the channels in the device. The middle layer is a 10 µm-thick polyester membrane with 2µm-diameter pores. The bottom layer, made from PDMS, houses the four basal channels that provide zone-specific access to measure TEER.

With these masks, a negative master is created on a polished silicon (Si) wafer (Fig. 3-5). SU8 3050 resist (MicroChem, Kayaku Advanced Materials Inc.) is spun onto the Si wafer at 900RPM for 30 seconds to create a 120um thick resist layer. The resist-coated wafer is baked for 10 minutes at 65 ˚C and then UV exposed (272 W, 45 seconds) to one of the masks. Once exposed, the wafer is subsequently baked at 95 ˚C for 30 minutes. The wafer is then developed in SU8 developer (MicroChem, Kayaku Advanced Materials Inc.) for 5 minutes, which removes any unpolymerized SU8 3050, rinsed with isopropyl alcohol, and dried with nitrogen gas. The wafer undergoes a final bake (2 hours, 125 ˚C) in order to release any mechanical stress in the patterned features, thereby improving their durability during PDMS molding.

The completed wafer is a negative master for PDMS molding via soft lithography. PDMS (Sylgar 184, Dow Corp.) is mixed in 10:1 ratio (base: curing agent), degassed and poured on top of the wafer. The wafer is then baked at 70 ˚C for at least two hours to cure the PDMS. After curing, the PDMS layer is peeled from the negative master and cut to size. Four mm diameter holes are punched using a punch needle to create inlets and outlets as shown on Figure 3-3. The negative master is reused for additional PDMS molding by repeating the process detailed above.

Once the top and bottom PDMS layers are completed, the final assembly can be performed. A porous membrane, described above, is exposed to oxygen plasma (Harrick Plasma, 30 W, 425 mTorr for 1 minute) and then submerged in 5% (3-Aminopropyl)triethoxysilane (APTES) at 80

˚C for 20 minutes. Membranes are then left to dry 2 minutes. While they are drying, the top and bottom PDMS layers are exposed to oxygen plasma (Harrick Plasma, 30 W, 425mTorr for 1 minute). This creates the necessary -OH groups on the PDMS surface that will bond to X on the surface of the membrane. The membrane is placed between the two PDMS layers and the layers are pressed to remove any air bubbles that may be at the interface. The PDMS assembly is heated to 100C for four hours to ensure irreversible bonding. The devices are thus completed and can be stored for months before being used for cell culture.

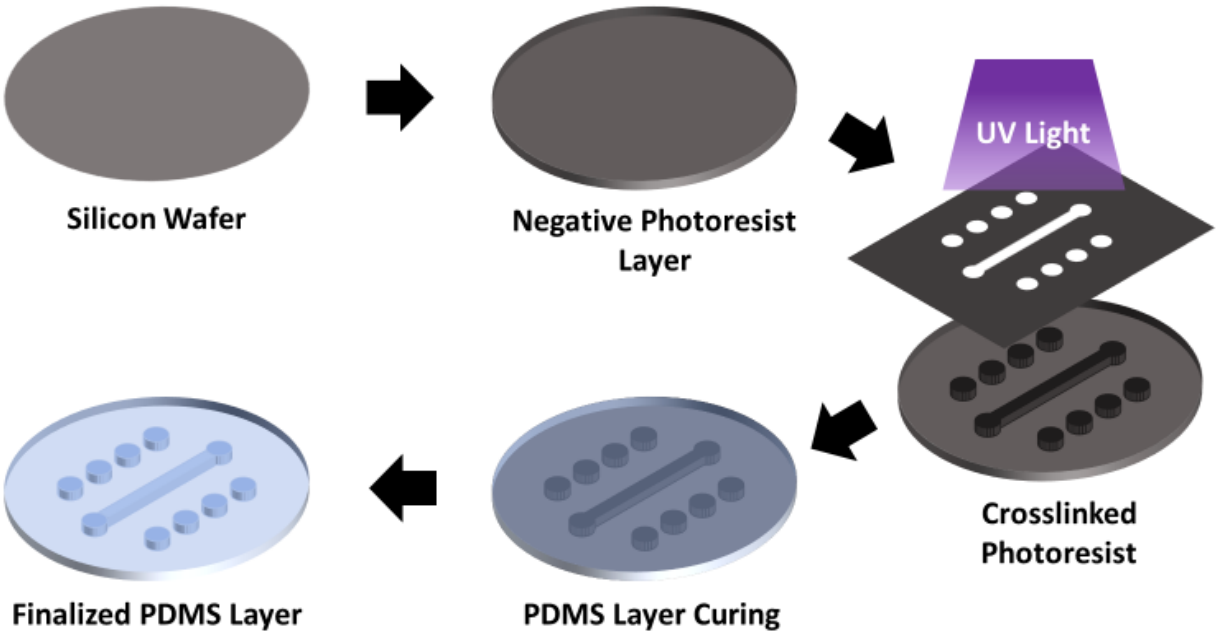

Figure 3-5 Fabrication process for mz-TEER. Photolithography is used to create a negative relief in negative photoresist on a silicon wafer. This master mold is then used for PDMS soft-lithography to fabricate the microfluidic devices. Each wafer can be used to make many devices by repeatedly mixing, pouring, curing, and peeling PDMS.

3.2.3 Computational Model

We developed a computational model using COMSOL Multiphysics to analyze the electrical impedance of various design prototypes and to validate experimental results obtained from completed devices. The electrical circuits models of COMSOL do not include the EDL, discussed in Chapter 2, thus providing a model equivalent to the mz-TEER four-probe setup.

In the model, shown in Figure 3-6, all the channels are filled with cell media with a conductivity of 1.6 S/m [49,50]. The cell monolayer is modeled as a 5um-thick layer with a conductivity of 1 mS/m, chosen to reflect those reported in the literature for an endothelial cell monolayer [28,51]. Electrodes are integrated in the model and have the same radius as the pins used in our electrode interface. We chose measurement parameters that we use with our platform, i.e. 12 Hz AC current with a 10 mV potential (EVOM2, World Precision Instruments, USA).

A key motivation for modeling is to inform us as to whether it would be necessary to normalize all impedance measurements to the changes in cell media conductivity that are a result of cell by-product accumulation during the 12-hour culture between each media change. We thus included a simulation in which the cell media conductivity varied 50%, 75%, 100%, 150%, and 200% of the expected value. In the next chapter, I will discuss the results of these simulations.

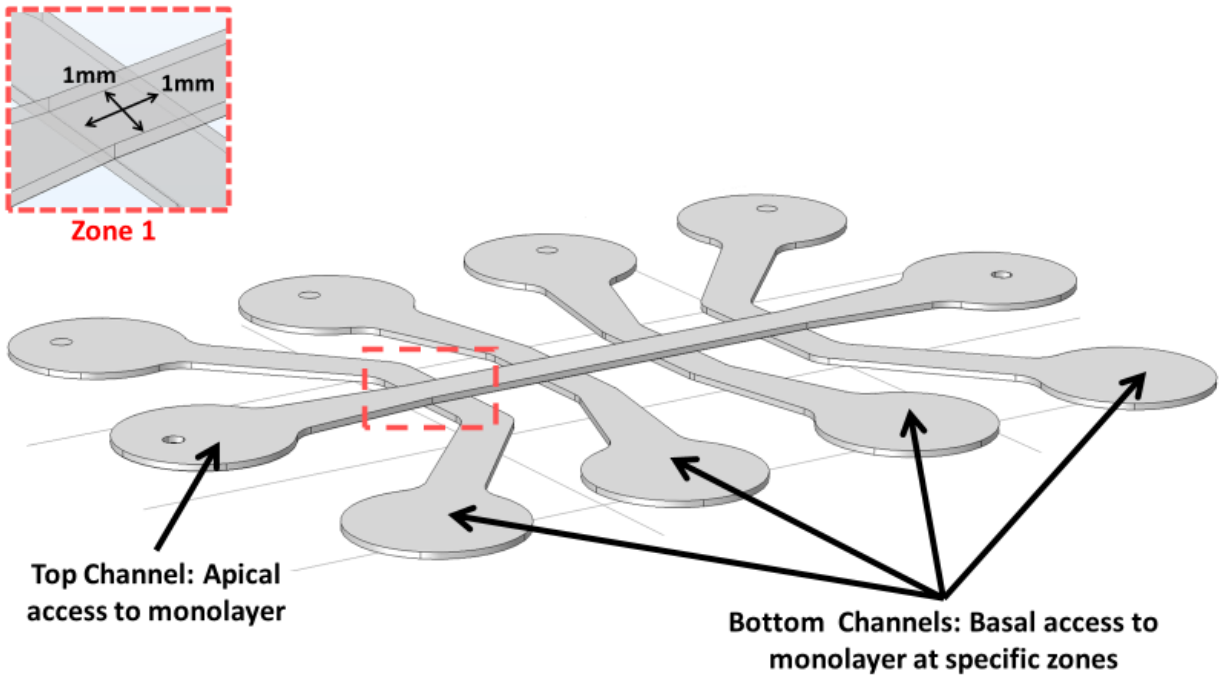

Figure 3-6 Three-dimensional view of the mz-TEER COMSOL model. The AutoCAD design used to fabricate our devices was imported into COMSOL to produce the model. Channel height is 150um. Arrows indicate the apical and basal channels, and inset shows a magnified view of Zone 1 with dimensions of 1mm x 1mm (W x L).

3.2.4 Electrode Interface

As mentioned previously, an attractive feature of our platform is the ability to perform four-probe measurements across various zones of an endothelial monolayer within the same device. We designed and fabricated a custom, reusable electrode interface that, when placed on top of the of the mz-TEER platform, connects to all necessary electrodes. This interface, shown in Figure 3-7, consists of a laser-cut acrylic sheet (75 mm x 23 mm, L x W) to which electronic pins (Sparkfun Electronics, USA) are inserted through cut holes and glued in place. The pins, which are connected to a custom circuit to be discussed in the next section, match the position of the inlets of the platform and can measure the monolayer in different zones. Overall, the benefit of having this reusable electrode interface is that a user is able to connect and disconnect to the platform quickly, which is important for media changes. The electrode interface can UV sterilized and be re-used with multiple devices.

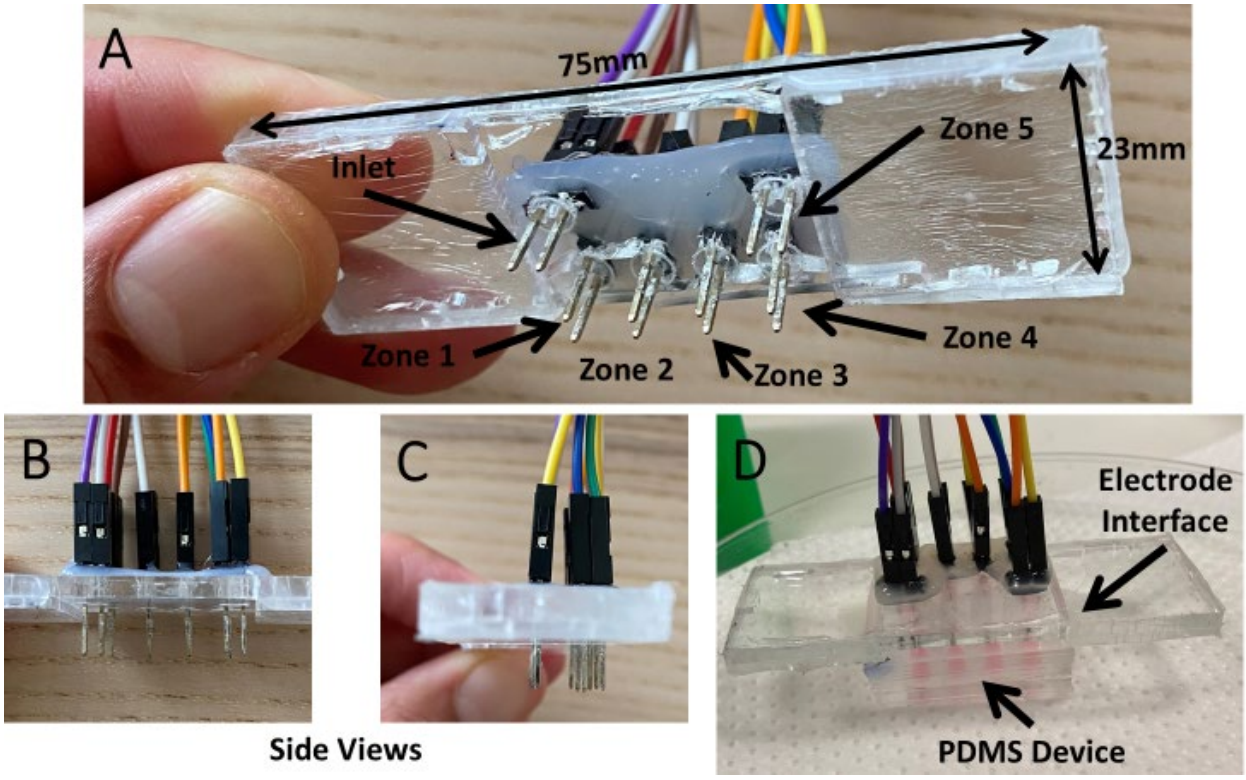

Figure 3-7 The electrode interface that connects to assembled mz-TEER devices. A, Dimensions of the interface and position of each electrode pair. B and C, Side views with electrodes extending 5mm from the interface. D, The finalized setup in which the interface is connected to a PDMS device and loaded into the incubator for measurements.

3.2.5 Hardware and Software

The custom electrode interface discussed in the previous section requires its own circuitry and software to operate. Specifically, it is controlled by an Analog Discovery 2 (AD2, Digilent Inc.), which produces an excitation signal and cycles through each zone of the platform, recording each impedance value. The AD2 uses in-house written software, which allows a user to enter the parameters for the excitation signal, how many cycles to run, and provide information about the device being measured. This software can be found in Appendix 8.2.

Attached to the AD2 is a custom circuit PCB that contains all of the necessary components to conduct four-probe measurements and the multiplexers needed to select each zone individually. This circuit, shown in Figure 3-8, has a single TEER measurement unit that by using two multiplexers, is connected sequentially to each of the five zones to record resistance values. This process cycles continuously until the user stops the measurements, resulting in a data log file containing the resistance data for each of the five zones.

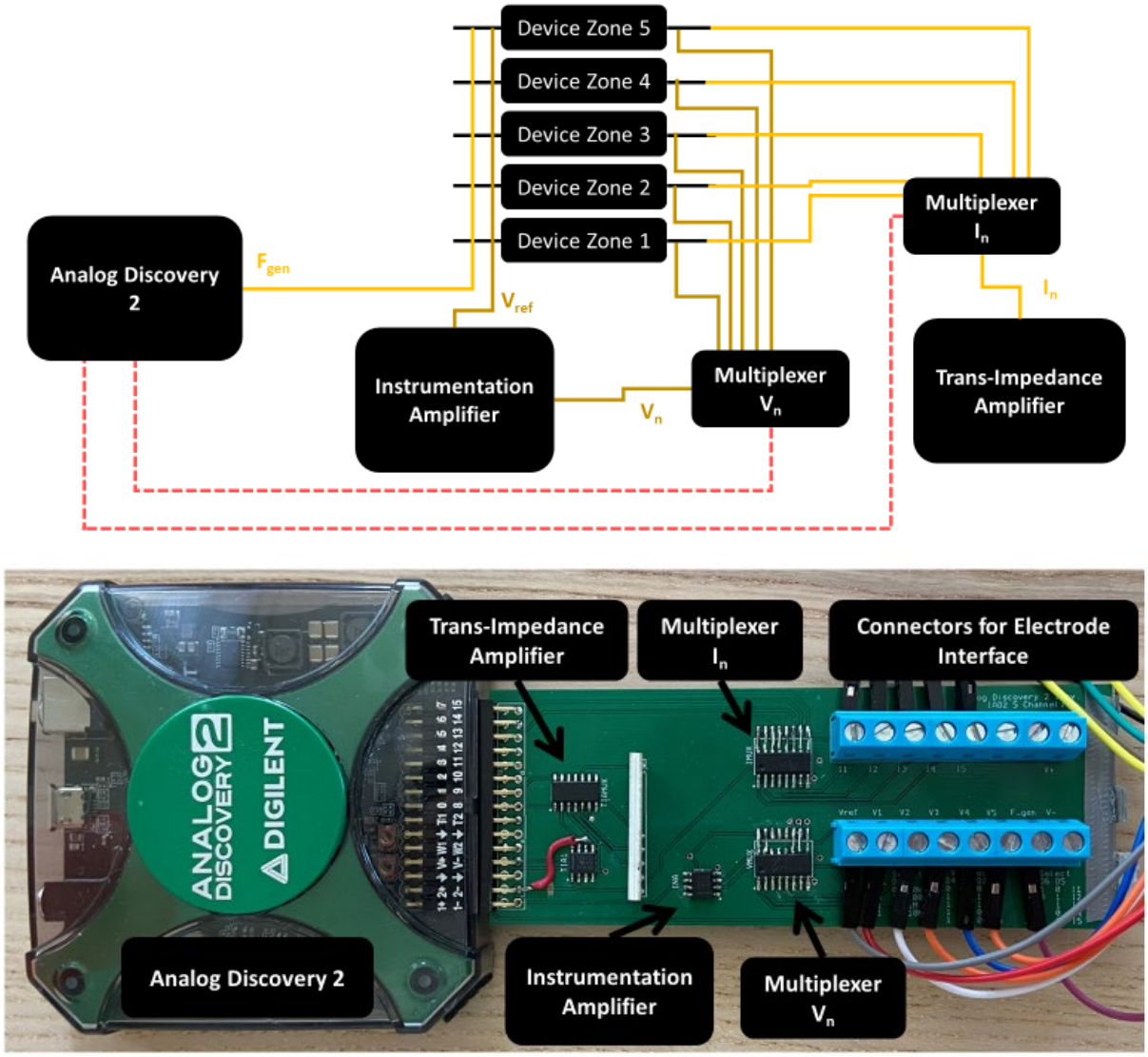

Figure 3-8 Electronic schematic and image of hardware that measures resistance in the mz-TEER platform. Components in the top schematic correspond to those on the custom printed circuit board in the image below. The Analog Discovery 2 (AD2) controller produces the potential applied across the monolayer and, using multiplexers, controls which zone is being recorded at any given time. The instrumentation amplifier (INA) measures the voltage and the trans-impedance amplifier (TIA) measures the current across a single zone. The zone's resistance is calculated (Equation 1) and recorded in a log file.

3.3 Experimental Methods

This section provides details regarding cell culture methods (traditional and in-device), the preparation of mz-TEER devices for experiments, and data acquisition and analysis.

3.3.1 Cell Culture

Cells are initially grown in flasks, usually, but not limited to, a T25 flask (Thermo Fisher Inc.). For the experiments I describe in Chapter 4, MCF7-GFP cells were chosen because fluorescent imaging is possible through the porous membrane. MCF7-GFP cells were cultured with Dubelcco's Modified Eagle Medium (DMEM) media supplemented with 10% fetal bovine serum (FBS) and 1% penicillin-streptomycin (PS), and were cultured in 37 ˚C in 5% CO2. Media changes were performed every 48 hours and flasks were split when confluency reached 80%. Only cells of less than Passage 15 were used.

To culture cells in the mz-TEER platforms, cells were prepared and loaded, as detailed in the next section. After loaded into the devices, the cells were maintained at 37 ˚C in 5% CO2. Because the volume of our devices is much less than traditional culture plates, media exchanges occurred every 12 hours as shown on Figure 3-9.

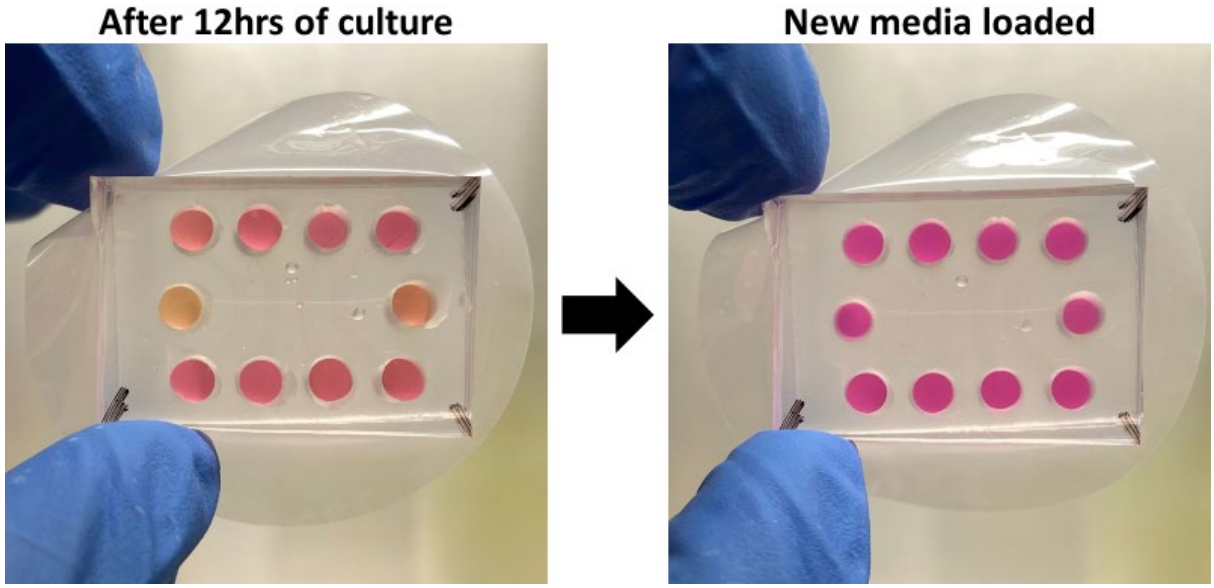

Figure 3-9 Images of mz-TEER devices before and after media changes. The total media volume in a device is 200 µL, and media was replaced every 12 hours to maintain cell viability. After 12 hours of culture, cell growth in the apical channel is confirmed by a stronger color change in the media in this channel. Media change frequency must to be optimized for different cell lines to ensure proper growth.

3.3.2 Device Sterilization and Cell loading

To sterilize devices, assembled mz-TEER devices are treated with oxygen plasma (Harrick Plasma, 30 W, 425 mTorr for 1 minute). This both sterilizes the device and makes the PDMS hydrophilic for easier loading of liquid. After plasma exposure, the devices are filled with sterile Phosphate-buffered saline (PBS) and exposed to UV light for 30 minutes inside a sterile bio-safety cabinet. After sterilization, the PBS is exchanged with cell media and the devices are placed in an incubator for at least an hour before cells are loaded (Fig. 3-10).

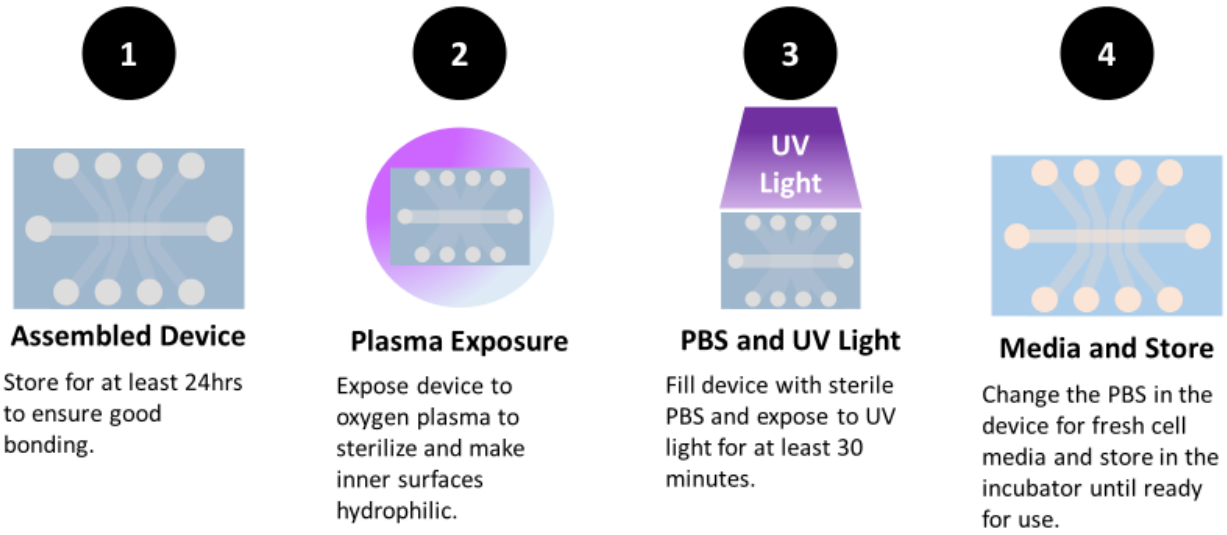

Figure 3-10 Schematic detailing the sterilization protocol. From left to right: the device is first assembled and stored for at least 24 hours to ensure proper bonding between the three layers. Subsequently, the device is exposed to oxygen plasma to sterilize and make surfaces hydrophilic. The device is then filled with PBS and exposed to UV-C light for 30 minutes, after which the PBS is exchanged for fresh cell media, and the device is stored in the incubator to equilibrate for at least 24 hours before cells are loaded.

During the time in which the devices are in the incubator, cell suspensions are prepared. Cells are released from their cell culture plate using trypsin. For a 25 cm^2 culture flask, 2 mL of 0.25% trypsin/EDTA is used for 5 minutes, and then neutralized with 4 mL of fresh media (2:1, media: trypsin). The suspension is centrifuged at 0.5 RCF and resuspended at a concentration of 500,000 cell/mL, which is sufficient to establish a monolayer in approximately 7 days. This timeframe is similar to that of Transwell Assays. Optimization (including seeding density and frequency of media changes) is needed to establish a monolayer in 7 days for other cell lines of interest. To load a device with cells, all of the cell media is removed from the top channel (apical), and 50 µL of the cell suspension is subsequently loaded. After allowing 5 minutes for the cells to settle, the inlet and outlet are filled with fresh cell media. This same procedure is used for media changes, where all of the media in the top channel is removed and replaced with fresh media.

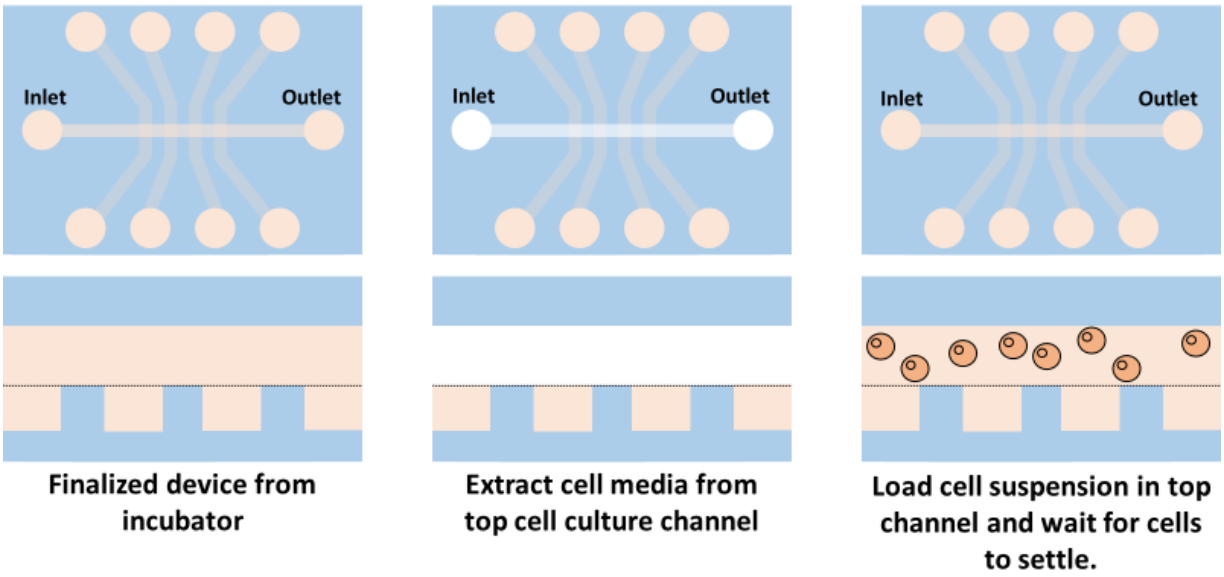

Figure 3-11 Schematic of the cell loading procedure. From left to right: the assembled and sterilized device is retrieved from the incubator and the media from the apical channel is removed using a pipette. The prepared cell suspension is then loaded into the apical channel, and cells settle and attach to the membrane during the 12 hours before the first media change.

3.3.3 Data Acquisition and Analysis

When cells are loaded into the device, the electrode interface discussed in section 3.2.4 is placed on top and the device is placed in the incubator. All of the data acquisition is controlled from a computer connected to the AD2. The user selects a file name, the duration of the measurement, and starts the software, which controls the AD2. TEER values for each of the zone is measured and stored in a log file.

Once measurements are completed, the data is analyzed using MATLAB or Excel. TEER values are normalized against that measured for zone 5. As discussed earlier, this normalization is key since it removes any changes in resistance caused by the variation in cell media properties. As will be discussed in the next chapter, this normalization also becomes important when chemical cues are introduced to disturb the monolayer and their effect on cell media conductivity needs to be accounted.

3.4 Discussion

In this chapter, I discussed the platform development process and the key design features met to create the mz-TEER platform. While we have included four zones of 1mm^2, using the same techniques we can easily reduce the area of each individual zone to accommodate for more zones and therefore achieve higher spatial resolution. In the next chapter, I discuss the platform validation, and experimental and computational simulation results.

4 RESULTS AND VALIDATION FOR MICROFLUIDIC-BASED MULTI-ZONE TRANS-ENDOTHELIAL ELECTRICAL RESISTANCE

Chapter Overview

In this chapter, I will discuss key results regarding cell loading and monolayer formation in the mz-TEER platform, zone-specific measurements, and how computational modeling aided platform validation and design guidance. Together these results demonstrate mz-TEER's capabilities, and the biological questions this platform can help to answer. Furthermore, I will discuss possible measurement sensitivity improvements, monolayer formation time optimization, and future work directions that would be interesting to explore.

4.1 Results

Here, I discuss important results regarding cell culture in the devices, results of the COMSOL simulations, the development of a normalization protocol, and mz-TEER results with MCF7-GFP monolayers.

4.1.1 Cell culture and Monolayer Formation

As shown in Figure 4-1, the formation of a confluent MCF-7-GFP monolayer was achieved in 168 hours (7 days). To test for monolayer stability, samples were kept in culture for seven more days and our fluorescent imaging confirms complete confluency even after fourteen total days. This is comparable with TA setups which take 1-2 weeks before a monolayer reaches complete confluency and is ready for TEER measurements[19,52]. The validation protocol we developed should be performed with any cell line that is going to be used, and if cell lines are not fluorescent, we recommend that cell tracer dye be used every 24-36 hours to monitor monolayer growth and formation.

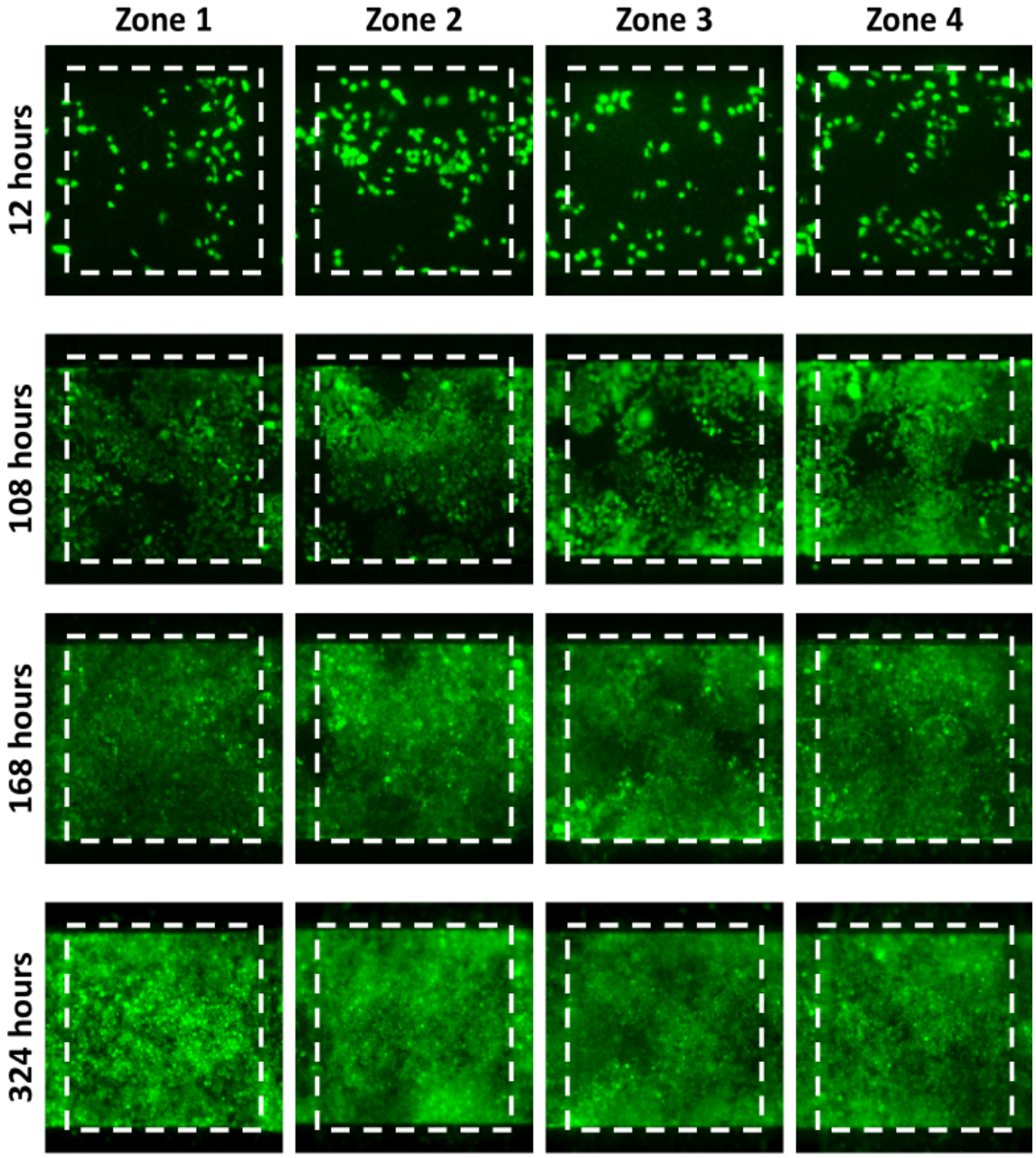

Figure 4-1 Micrographs of an MCF-7GFP monolayer in the mz-TEER platform. Media changes were conducted every 12 hours and fluorescent images taken every 24 hours, beginning 12 hours after seeding cells. White dashed lines outline the zone perimeter (L =1 mm and W =1 mm).

4.1.2 COMSOL Simulations

To validate our measurements of each specific zone, we employed the COMSOL model discussed in the previous chapter. Shown below are the results obtained from these simulations in which the measurement of each zone is simulated with an applied potential of 10 mV. The streamlines for the electric potential are plotted in red and show the path of the current along the device for each of the measurement zones. These data validate the mz-TEER design by demonstrating that during each zone-specific measurement, the current only crosses the monolayer—from top apical channel toward the bottom basal channel—through the intended zone of interest as shown on Figure 4-2.

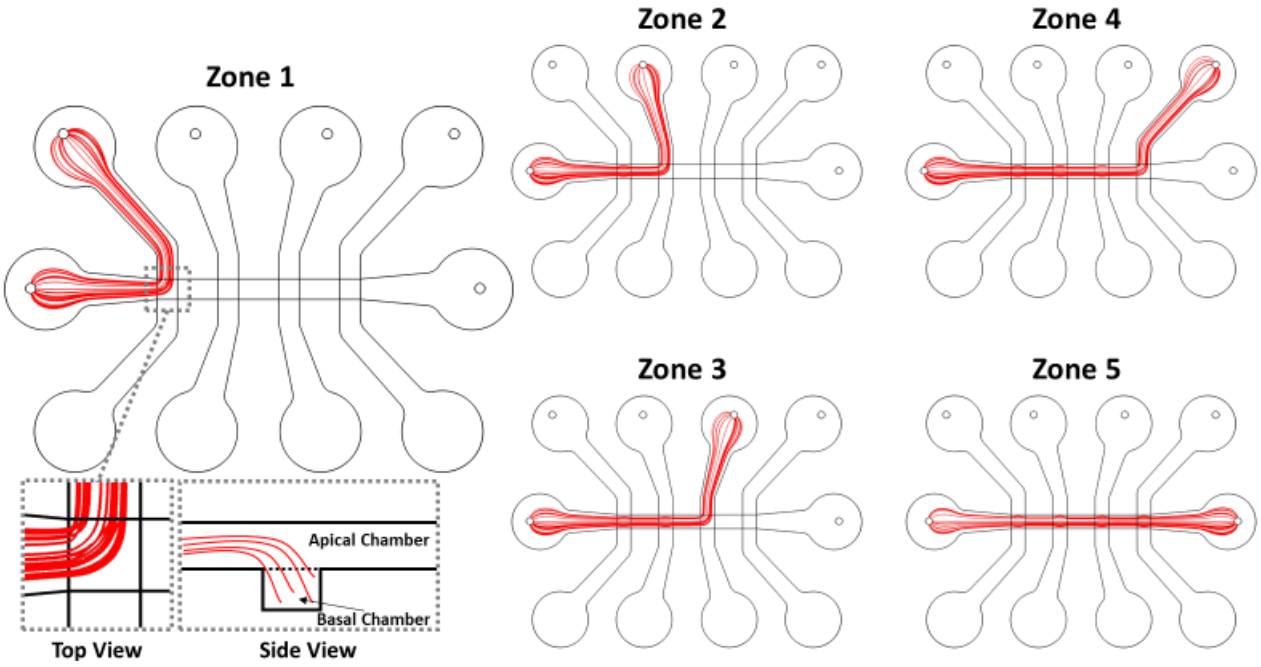

Figure 4-2 COMSOL mz-TEER simulation results. The electric potential distributions, shown in red, confirm zone specific measurements by passing only through the measurement zone of interest. Top view inset shows a magnified view of the distribution when measuring zone 1, and the side view inset illustrates how the potential crosses through the zone.

Results from these simulations are graphed in Figure 4-3. Figure 4-3 A shows that indeed changes in media conductivity will affect our zone-specific measurement, and that these changes are also observed in zone 5 (the cell media monitoring zone), which we can use to normalize. Panel B shows how the resistance of zone 2 when normalized against the resistance of zone 5, resulting in the elimination of measurement changes as a result of media conductivity changes discussed in the previous Chapter. In Panel C, we normalize the data for all zones with respect to zone 5 to determine the expected normalized resistance value for each of the zones. As expected, and shown in Figure 4-3, the baseline resistance increases from zone 1 to 4 since microfluidic channel between the electrodes is longer (see Figure 4-2). Panel D shows that the normalized resistance of each zone is 14% higher when a cell monolayer is included in the simulation.

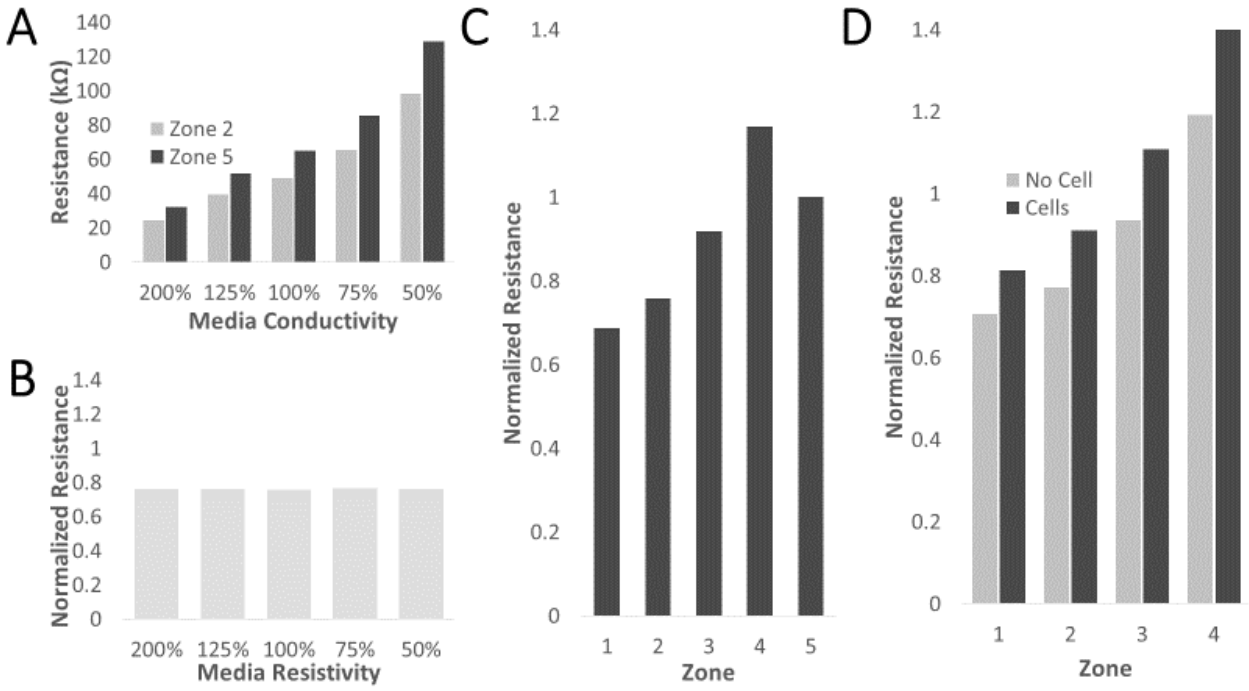

Figure 4-3 Data normalization testing using COMSOL simulations. A, Shows the resistance values for zone 2 and 5 as a function of media conductivity (100% represents the nominal value for media conductivity, 1.6 S/cm). B, Confirms that normalizing to zone 5 removes the effects of media conductivity, thus allowing the platform to detect only changes in the monolayer (simulated normalized resistance for zone 2). C, Normalized resistance for all zones. D, Expected normalized resistance values with and without cells based on our simulations.

4.1.3 Hardware Validation with Calibrated Resistors

Prior to mz-TEER measurement, we first validated the hardware setup and software. We used various resistors with known values and measured the circuit when connected to each of the zones. Resistors, ranging from 990 Ω -98.5 kΩ, were employed in order to test the dynamic range of the platform. A maximum resistance measured in our devices, however, was 45 kΩ. Based on this data (Fig. 4-4), the maximum error we see is 1.1%, which is within the minimum expected change in resistance of 14% when cells are loaded based the results discussed in the previous section.

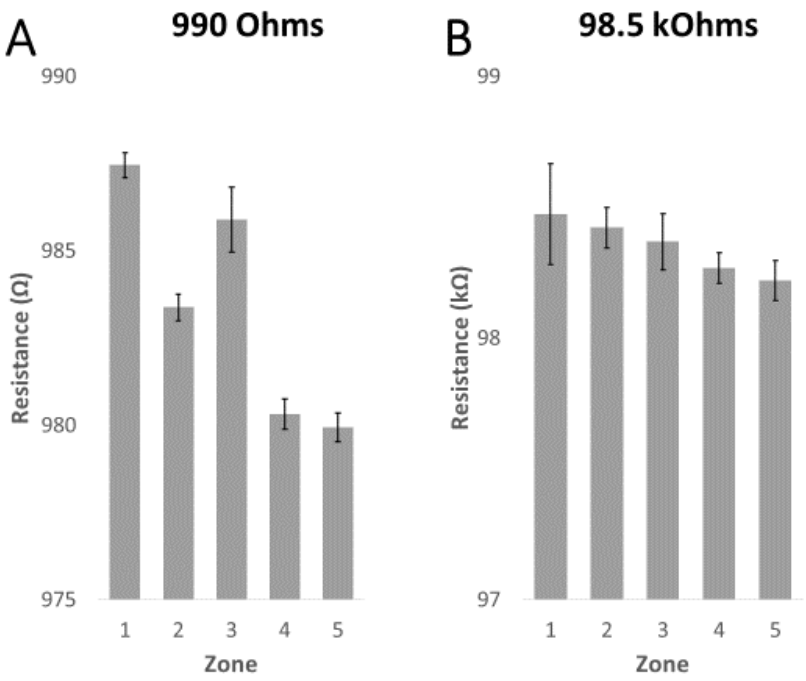

Figure 4-4 Characterization of the AD2 and custom electronics. A, A 990 Ω resistor was measured using electrode pairs for each zone for validation. The highest error measured was in zone 5, a 1.1% difference from the nominal resistance. B, The experiment was repeated with a 98.5 kΩ resistor, with zone 5 having a 0.3% difference. n=10 for all measurements, and error bars indicate one standard deviation.

4.1.4 Measurement Time Optimization

To ensure the highest sensitivity in our measurements, we investigated whether the "cycle" time, the time it takes to perform a measurement in each zone, limits the temporal resolution of our platform. To determine the minimum cycle time that can be achieved, a range of measurement times were tested and their corresponding coefficient of variation (CV) was compared. A device with no monolayer was setup inside an incubator and measured. Fifty measurements taken of each zone using cycle times of 1, 2, and 4 seconds, after which the CV was calculated for each data set. As shown in the Figure 4-5, our results show that there were no differences between cycle times of 1 and 2 seconds but a significant increase in the CV for the 4 second cycle time. Based on these tests, we choose a cycle times of 1 second, which was also the lowest, and correspondingly, the highest temporal resolution that is achievable with our current setup. It is important to note that with cycle time of 1 second, when we include the measurement of each zone sequentially and the operation of the multiplexers, zones are measured every 15 seconds.

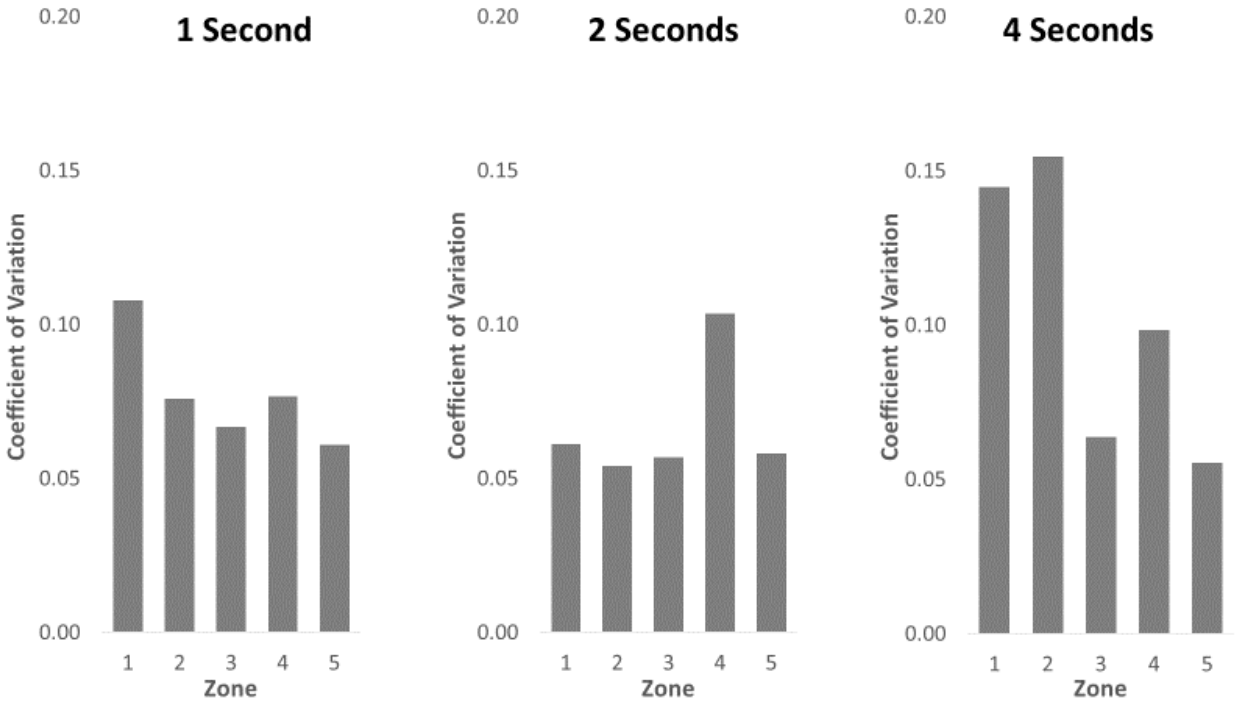

Figure 4-5 Comparing the effects measurement time on the measured resistance at each zone. A device filled with cell media and kept at room temperature, was measured 50 times (50 data points per zone) and the CV calculated for each zone. The measurement time was changed in the software (1, 2, 4 seconds).

4.1.5 Normalization and Stability of mz-TEER Measurements

Since changes in TEER should correspond to changes in endothelium properties, we wanted to ensure that our platform is stable and robust. Computational models, as discussed, showed that we should normalize our TEER measurements in each zone by zone 5, which again measures the conductivity changes of the cell media. To test this normalization on our platform, we exposed a control device (no cells) from 22 ˚C(room temperature) to 37 ˚C(incubator) for 5 minutes and again to 22 ˚C, and recorded mz-TEER. As shown in Figure 4-6, media conductivity changes are indeed captured by our measurements.

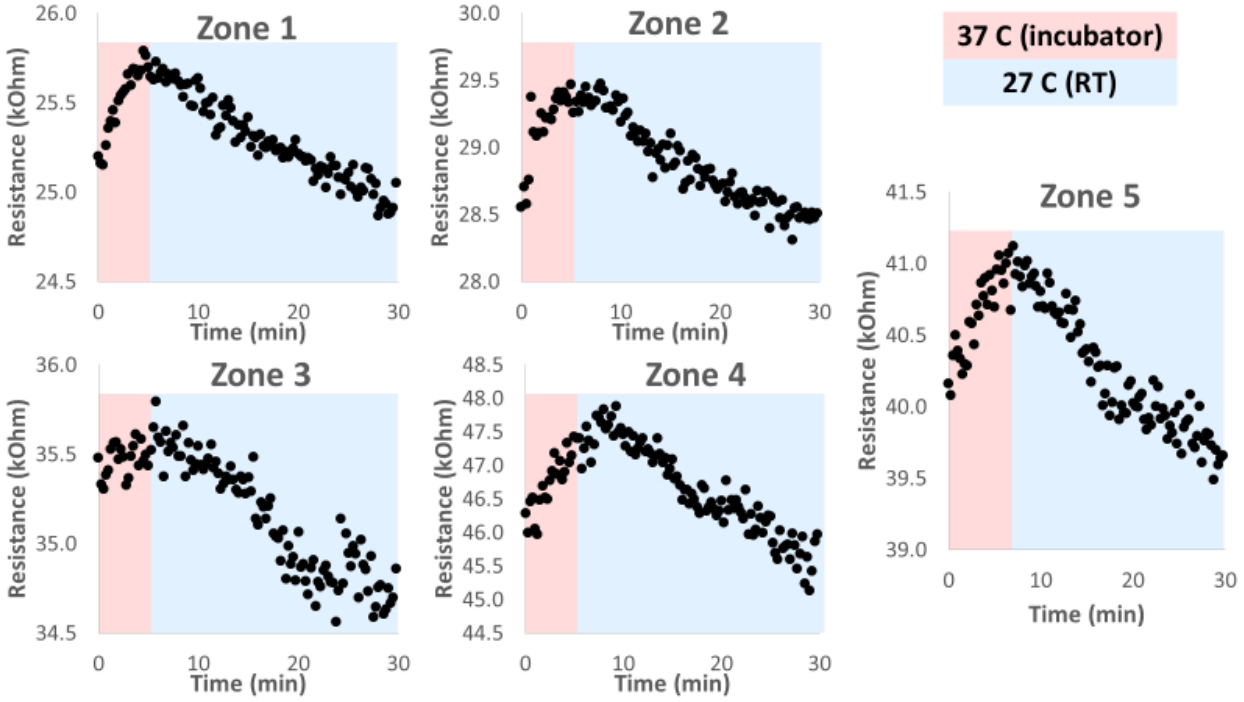

Figure 4-6 Resistance normalization validated by varying temperature to change cell media conductivity. Resistance was measured for 30 minutes with devices filled with cell media. Devices were placed in an incubator for 5 minutes (pink region) then removed and maintained at room temperature (blue region). The change in media conductivity is apparent in all of the zones.

Using the data in Figure 4-6, each zone is normalized against zone 5, and Figure 4-7 shows the differences in CV between normalized and raw data. Overall, these data show that not only is normalization is a good approach to remove any variability due to the cell media, but also our measurement platform is indeed stable and robust.

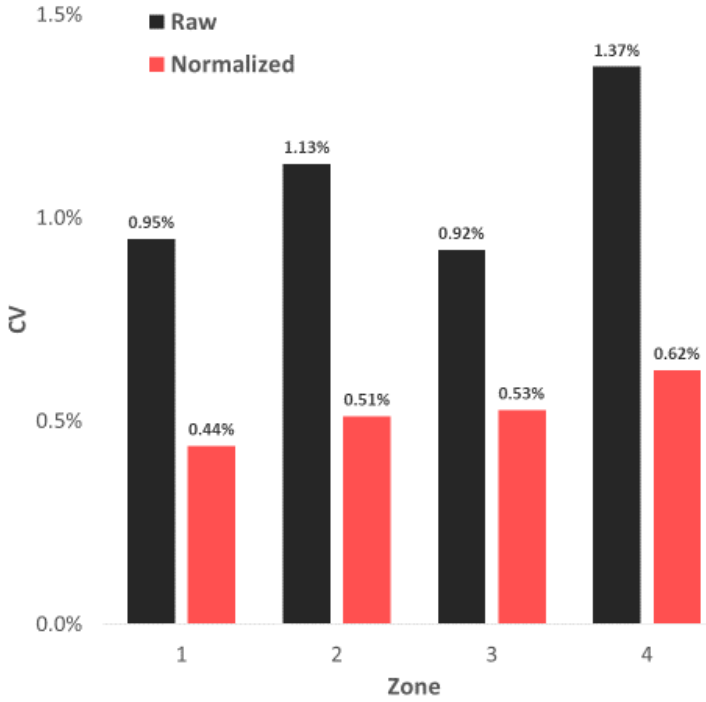

Figure 4-7 Coefficient of variation of raw versus normalized mz-TEER measurements. Normalization reduced the CV for all zones, with zones 1 through 4 decreasing by 54%, 55%, 47%, and 55%, respectively. To calculate CV, the standard deviation was divided by the mean. For all zones, n=120.

4.1.6 Baseline Resistance for mz-TEER Devices

In this section, we evaluate the baseline resistance of our devices, and test if electrode interface placement has any effect on our measurements. Figure 4-8A shows the normalized resistance of control (no cell) devices against the COMSOL showing no statistical significance.

Another importance regarding baseline values, because we are connecting and disconnecting the electrode interface for media changes, we were concerned whether this introduces variability to our measurements. To investigate this, we set a control (no cells) device inside the incubator, performed a mz-TEER measurement, took the device out to replace with fresh media, placed the device back in the incubator, and measured mz-TEER. We repeated this a total of seven times. The variation introduced is quantified in Panel B, where we show that the maximum coefficient of variation is 7% (zone 1) which is within our 14% limit as described in Section 4.1.3.

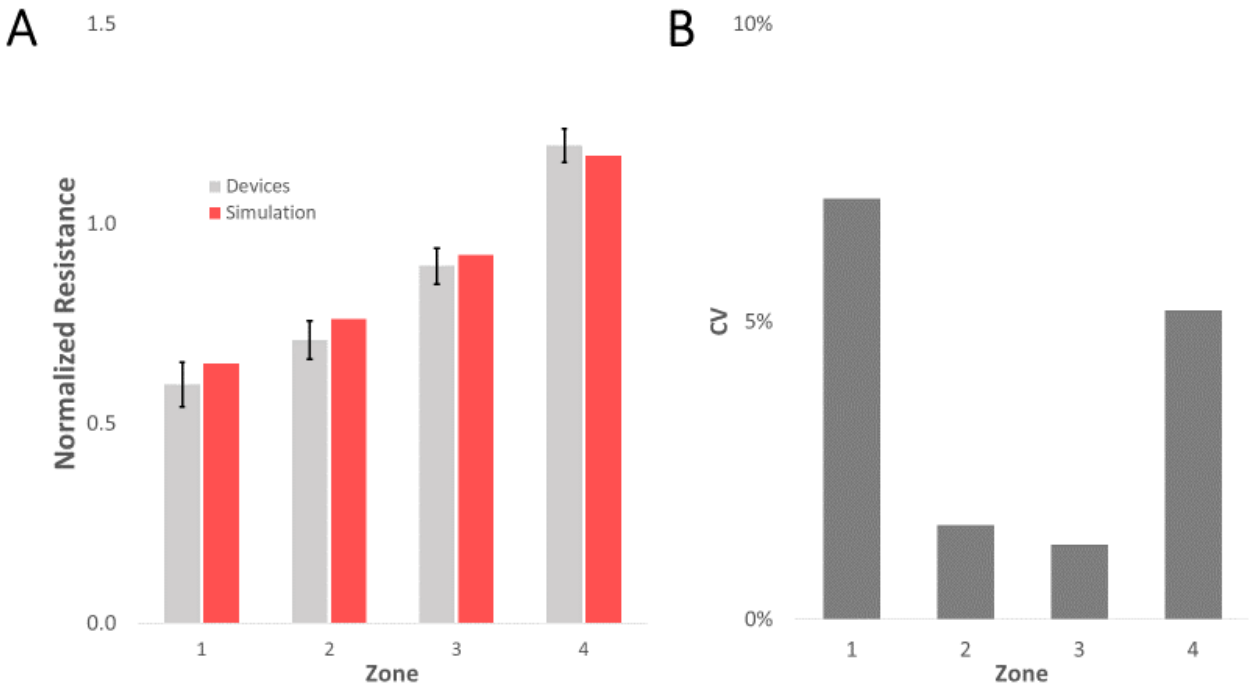

Figure 4-8 Baseline NR values for mz-TEER devices. A, Comparison of the baseline NR for devices (n=60) with COMSOL results, with no significant difference (Student's t-test). B, Maximum CV was 7% (Zone 1) after seven media changes. Devices were placed in the incubator and mz-TEER was measured. Devices were then retrieved, the media replaced, and the process repeated a total of 7 times.

4.1.7 mz-TEER Measurements During Long Term Cell Culture

To validate our platform's capability of long-term cell culture and continuous mz-TEER measurements, we measured and compared unloaded (control) and loaded (monolayer) devices. The conditions of both these devices were the same, and all of the media changes were performed every 12 hours. mz-TEER measurements were taken 30 minutes after each media change to ensure that the media temperature and CO2 concentration reached steady state once the devices were placed back into the incubator.

Shown below are the results of the unloaded devices. In general, all of the zones follow their expected normalized resistance (NR) value and remain stable during the 288 hours (12 days) of experimentation. Deviations in NR at hour 216 (zone 1) and hour 240 (all zones) and hour 216 (zone 1) are a result of air bubbles introduced into the channels during media exchange. Since PDMS is gas permeable, the air bubbles eventually escape, as shown by the next data point (e.g. hour 252). To test that our signal is stable, we compared the first five datapoints against the last five via a Student-t test. Shown on Figure 4-9B, we determined that there was no statistical significance between the two, thus suggesting that our baseline measurements without cells are stable.

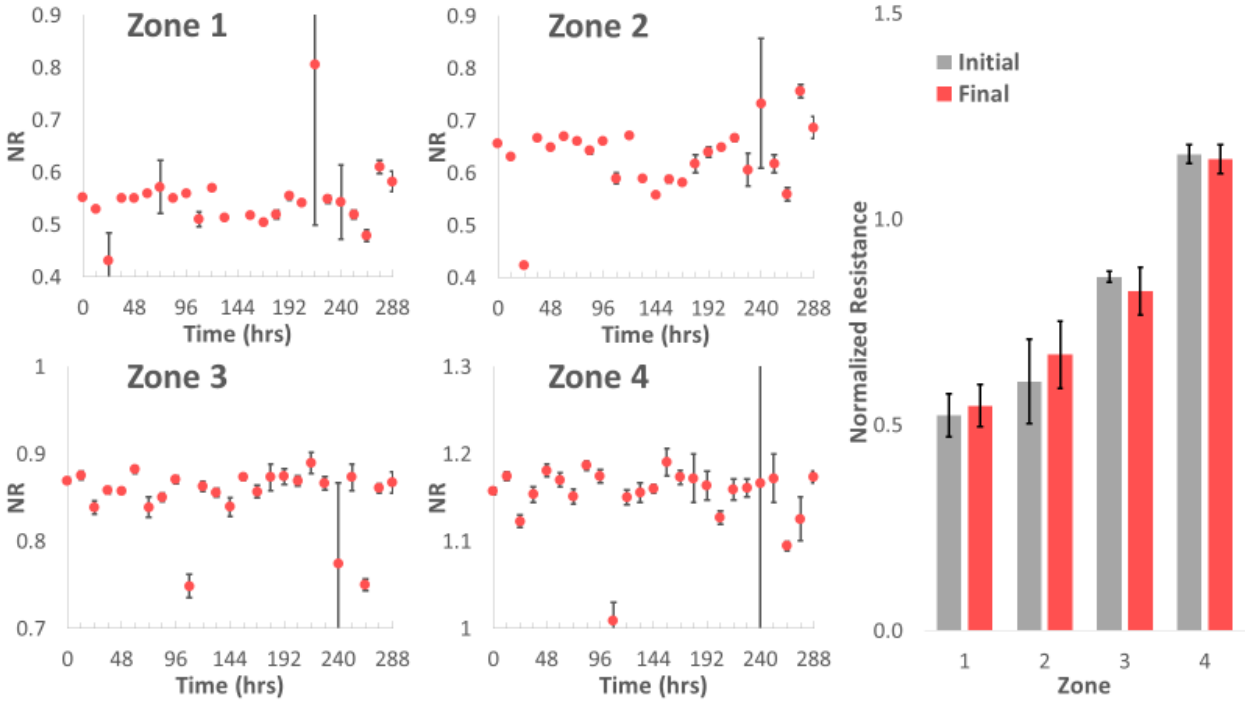

Figure 4-9 Long-term mz-TEER measurements on control devices (no cells). Devices were cultured for a total of 14 days and media changes performed every 12 hours. Scatter plots show NR values for zones 1 through 4 (n=10 for each data point; error bars represent one standard deviation). The bar graph compares the initial and final five measurements of each zone (n=5 for each bar; error bars represent one standard deviation). Differences between initial and final values for each zone were not statistically significant (Student's t-test).

Figure 4-10 shows the data we obtained for a device in which cells were loaded at time t = 0hrs. As seen on the graphs, we do not observe the expected rise of normalized resistance due to the monolayer barrier function. Performing a statistical comparison between the first five values we measured and the final five, we find that there is no difference between the values. It is possible that the rise in normalized resistance (NR) that we would have expected to measure was masked by variability introduced with an electrode-interface alignment issue or the accumulation of cell by-products in the porous PDMS.

Another possible reason for this lack of resolution could be because measurements where performed every 12 hours. In the following sections, we will discuss results which showed that we were able to measure barrier function successfully. These results suggest that measurement frequency is important.

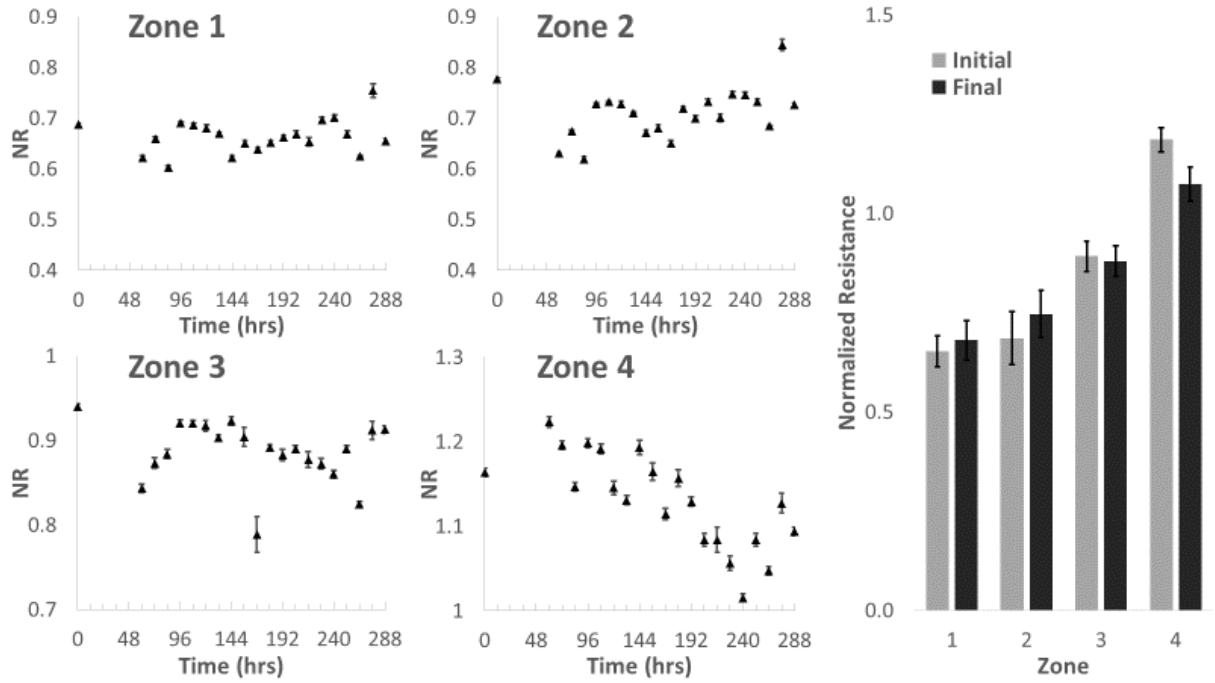

Figure 4-10 Long-term mz-TEER measurements on devices with a MCF7-GFP monolayer. Devices were cultured for a total of 14 days with media changes every 12 hours. Scatter plots show NR values for zones 1 through 4 (n=10 for each data point; error bars represent one standard deviation). The bar graph compares the initial and final five values of each zone (n=5 for each bar; error bars represent one standard deviation). Differences between initial and final values for each zone were not statistically significant (Student's t-test).

4.1.8 Determining mz-TEER Dynamic Range by Perturbing the Monolayer

In this section, we present our findings on real-time monolayer perturbation. With this experiment, we determined the dynamic range of mzTEER in the presence of an endothelial monolayer. We used trypsin to disassemble the monolayer and subsequently removed all the cells from the device. Using the devices from the previous section, after 14 days of culture, we measured a loaded (monolayer) and an unloaded (control) device. Media in each device was replaced with 0.25% trypsin/EDTA, and the device placed inside the incubator with measurements taken for 30 minutes. Shown in Figure 4-11 are the results: red data points represent control (no cells), and black represent loaded devices.

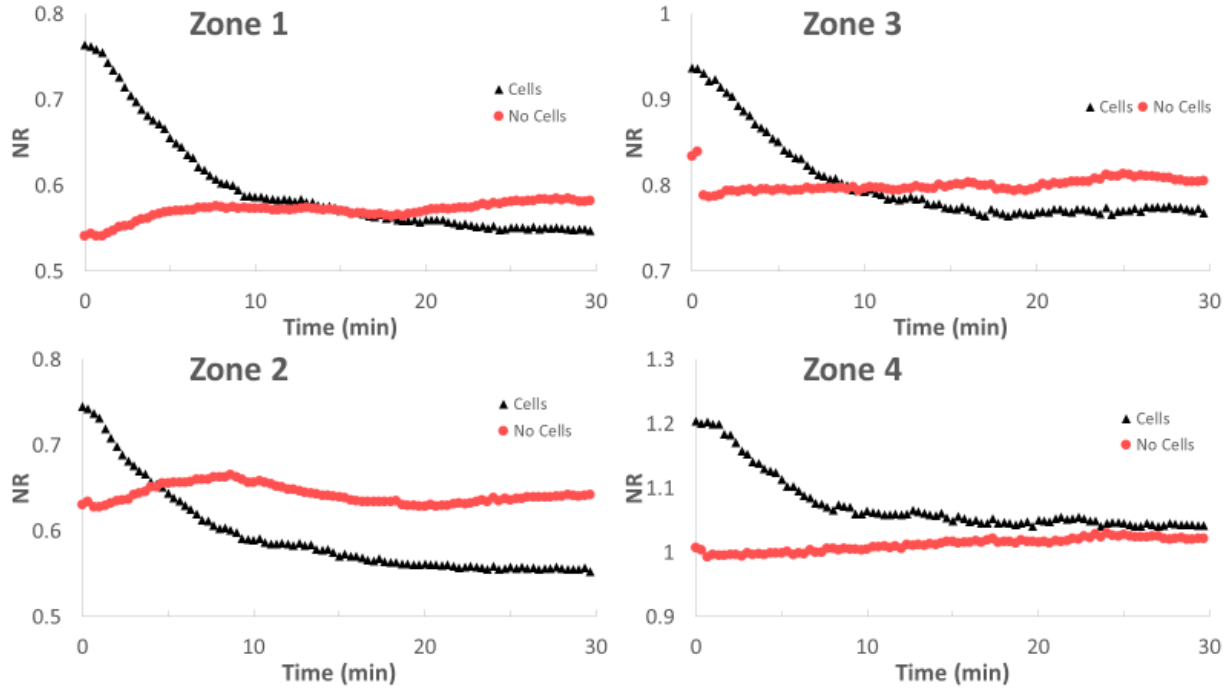

Figure 4-11 Dynamic range of mz-TEER using 0.25% trypsin/EDTA to dissociate MCF-7GFP monolayer. Both devices were cultured for a total of 14 days with media changes every 12 hours. After 14 days, the media was replaced with trypsin solution and mz-TEER measurements taken every 15 seconds inside an incubator. The NR for control devices is indicated in red, and the NR for loaded devices is indicated in black.

For all the zones shown in Figure 4-11 the decrease in NR due to trypsin-induced cell dissociation is observed within the first ten minutes. The effect of trypsin on the monolayer in each zone is confirmed with fluorescent imaging (Fig. 4-12). After the first ten minutes, when all the cells have been dissociated, the NR value stabilized and remained constant, like the control devices (shown in red).

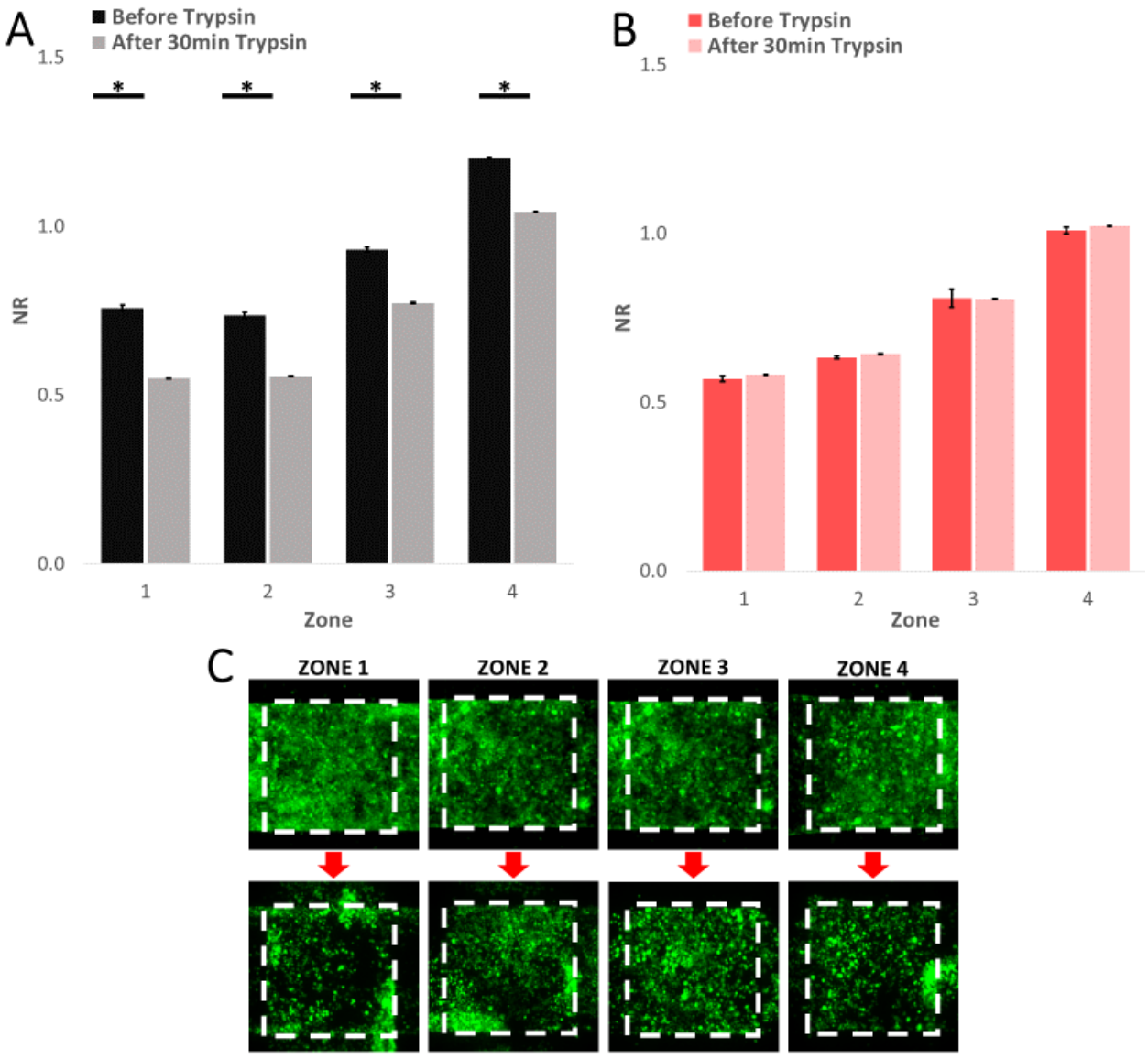

Figure 4-12 Comparing mz-TEER measurements on control and loaded devices after trypsin exposure. A, Bar graph comparing the NR values 1 minute and 30 minutes after treatment with 0.25% trypsin for an mz-TEER device with an MCF7-GFP monolayer. B, Bar graph comparing the NR values 1 minute and 30 minutes after treatment with 0.25% trypsin for a control device. C, Micrographs of an MCF-7GFP monolayer (zones 1-4) before and after 30-minute trypsin exposure. For all zones and conditions, n=5; error bars represent one standard deviation. * denotes $p < 0.05$ (Student's t-test).

4.1.9 Viability Testing of Long-term Continuous mz-TEER Measurements

To determine whether the platform and cells are capable of long-term continuous mz-TEER measurement, we ran a 14.5-hour long experiment, starting when the cells are loaded followed by TEER measurements every 15 seconds. The data, shown below in Figure 4-13 suggests that the platform is capable of long-term measurements. Zones 3 and 4 show relatively constant TEER values, which we hypothesize is due to the higher impedance baseline masking any small changes. For Zones 1 and 2, the NR has a sharp decrease after the first media change (indicated by the dashed lines) suggesting the introduction of an air bubble, as discussed on section 4.1.7. Altogether, this preliminary data suggests that long-term continuous mz-TEER measurements are possible. Further experiments are needed with mz-TEER devices that contain a confluent monolayer to evaluate the sensitivity of this approach to detect differences between zones.

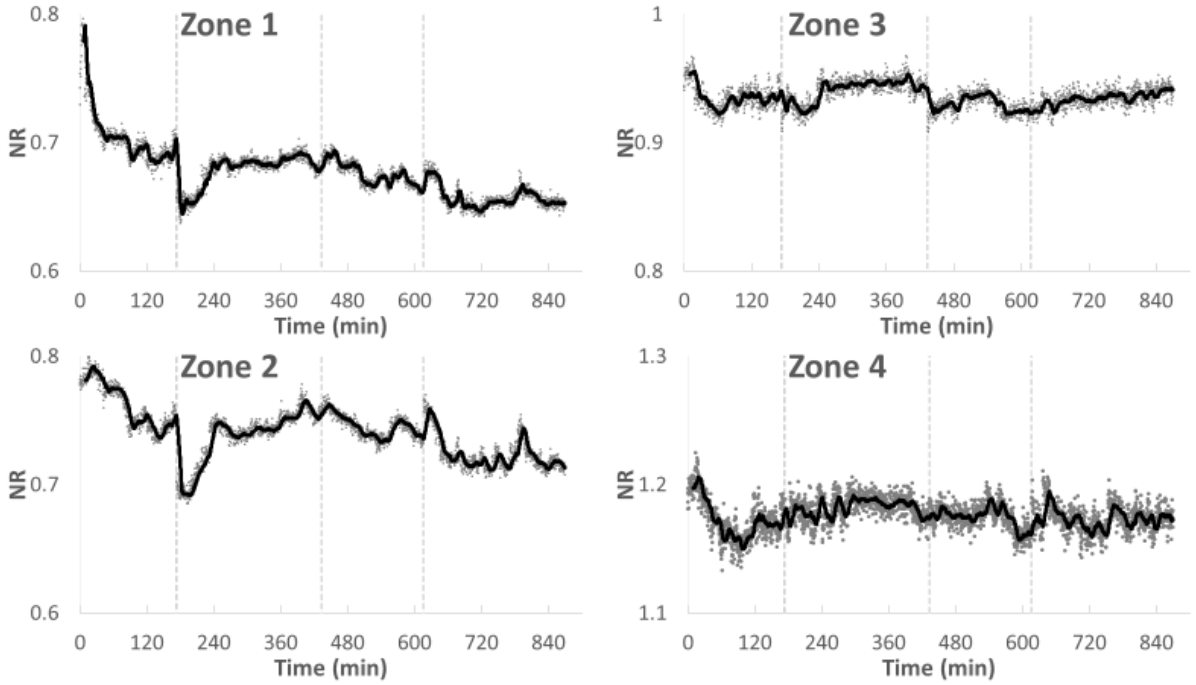

Figure 4-13 Long term continuous mz-TEER measurements. MCF-7GFP cells were loaded at t = 0 min, and the device was placed in the incubator. mz-TEER measurements were taken every 15 seconds for a total of 14.5 hours. Dashed lines indicate media changes, and the solid black line represents a moving average of 30 measurements (7.5 minutes).

4.2 Discussion and Future Work

mz-TEER is a novel platform that offers spatiotemporal resolution of TEER measurements. Using lithographic techniques to create a two-layer PDMS device with a porous membrane in the middle, we could integrate multiple measurements zones within a sample, something of which was not possible previously. Our new platform required the development of custom electronics that enabled four-probe impedance measurements in the 5 zones. Improvements to the platform include: performing frequency sweeps on each of the zones, which would yield more information about the monolayer, and creating an electrode-interface that enables cell media changes without having to disconnect the interface from the device. The latter would greatly improve the reliability of our measurements, as discussed in section 4.1.6.

A key aspect of the mz-TEER platform is the ability to culture cells until monolayer formation, which takes approximately 14 days. The capability of long-term culture in our device is characteristic of a well-designed device that considers the needs of cells, not only to survive but to form a healthy monolayer. The experiments presented here attest to our platform's capability to grow monolayers and to probe them in various ways. A key aspect of our design that was not tested, and should be a focus of future work, is zone-specific perturbations. As discussed on 4.1.2, the platform provides zone-specific basal access, which can be used to introduce certain cues to specific zones and study the spatiotemporal reaction of the monolayer. Does the perturbation remain in a single zone? Is the messaged relayed along the monolayer? These are questions this platform can uniquely answer. Another application that should be explored is to test whether the current spatiotemporal resolution is sufficient to study cancer cells undergoing trans-endothelial migration (TEM) across the monolayer. This would be a novel non-invasive approach to capture such phenomena. Refinement to the platform include reducing the area of each zone measure, which would reduce the cell-cell junctions being monitored at once.

In general, mzTEER represents the next-generation TEER measurements and will enable scientists to better test and understand monolayer behavior, and in turn, improve our understanding of the endothelium.

5 MULTI-ZONE IMPEDANCE MEASUREMENTS FOR VISCO-NODE-PORE SENSING

Chapter Overview

In this chapter, I will discuss my work toward single-cell viscoelastic measurements. This proof-of-concept platform, which I refer to as multi-zone viscoNPS (mz-viscoNPS), employs a multi-zone impedance measurement to enable interrogating a single cell at multiple frequencies. This improvement would provide much more detailed mechanical properties for each cell, thus improving stratification of cells from different populations or subpopulations. I will delve into the details of developing this proof-of-concept platform, the preliminary testing of this platform, and discuss why a multi-zone approach is a viable solution.

5.1 Introduction

Understanding cellular mechanical properties, especially at the single-cell level, can elucidate various biological mechanisms and functions [14,29,44]. Cellular mechanical properties arise from intracellular components such as the cytoskeleton and nucleus[29,53–56]. Differences in these properties have been linked to various biological processes such as metastasis and cell division[10,29,57,58]. Traditionally, cellular mechanical properties are measured with atomic force microscopy (AFM) or micropipette aspiration[59–62]. Although they represent the gold standard in the field, these techniques require a complex experimental setup and can only process a few cells per hour[10,44,63].

To overcome these drawbacks, the Sohn Lab developed visco-Node Pore Sensing (viscoNPS), a microfluidic platform that measures the viscoelastic properties of cells. As outlined in Chapter 2, the visco-NPS platform consists of a microfluidic channel segmented by nodes. One segment, the contraction channel, is narrower than the diameter of the measured cells and is sinusoidal in shape. Consequently, a cell that transits this segment is periodically squeezed. A current pulse is measured using a four-probe measurement. This pulse is sinusoidal, reflecting the periodic deformation of the cell. Information on the cell's elasticity (G') and viscosity (G") can be extracted from the current pulse (Fig. 5-1)[29]. In this chapter, we examine a proof-of-concept design that integrates a multi-zone approach to measure the resistance of multiple contraction channels in series. This will directly result in multi-frequency single cell viscoelastic measurements.

To achieve this, we employ techniques and knowledge gained from developing mz-TEER (Chapters 3 and 4) to modify the current viscoNPS platform design to enable multi-zone measurements. The following sections describe the microfluidic design, development of hardware and software, and preliminary results of devices with two, or four zones. These results serve as a blueprint for future work, and we detail key next steps to improve the platform's capabilities.

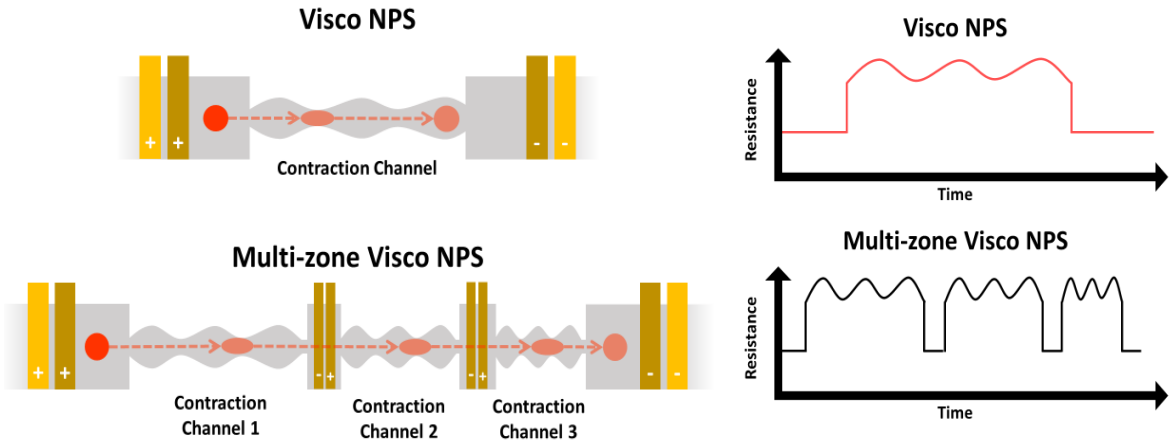

Figure 5-1 Schematic comparing viscoNPS and the proposed multi-zone viscoNPS. Left: multi-zone viscoNPS uses two extra pairs of electrodes to monitor the resistance in the second and third contraction channel. Right: expected resistance pulses from corresponding schematics on the left. For a single cell passing through the channel, the proposed multi-zone approach would produce three pulses corresponding to the measurement at each of the three contraction channels (each with a distinct frequency).

5.2 Platform Design and Fabrication

This section includes details about the design process, design considerations for multi-zone measurement, the platform fabrication, and the hardware and software developed.

5.2.1 Microfluidic Design and Fabrication

Our platform consists of two parts: the PDMS channel, which includes the sinusoidal contraction channels, and the glass substrate with patterned electrodes, which provide an electrical interface for each zone. The AUTOCAD design of a four-zone device is shown in Figure 5-2, where the PDMS mold and electrodes are represented in red and yellow accordingly. For the device designed to measure MCF-10A cells, the contraction channel geometry follows the sinusoidal equation presented in Figure 5-2 [29].

An example of an assembled device is presented in Figure 5-3.

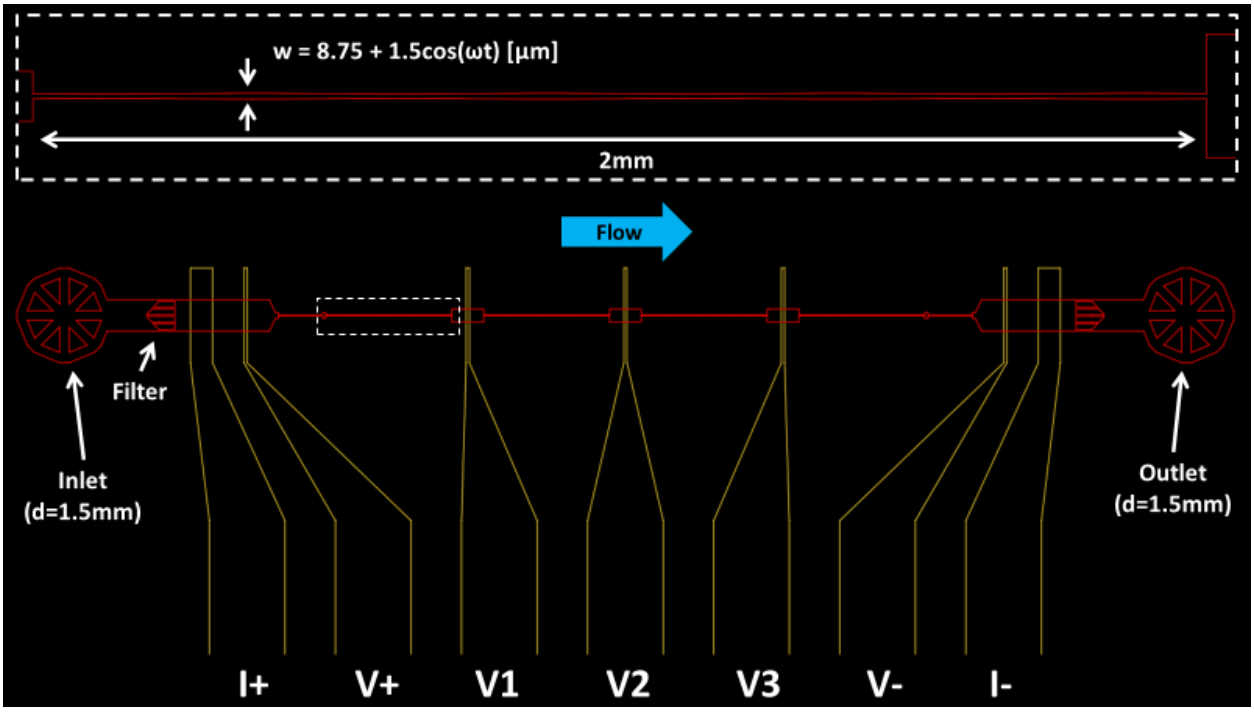

Figure 5-2 AUTOCAD design for a multi-zone viscoNPS device. Inset shows close-up view of the first contraction channel (white dash line). The contraction channel is sinusoidal in shape, containing four periods and a peak-to-peak amplitude of 3 μm. Yellow lines indicate the position of each electrode within the microfluidic channel.

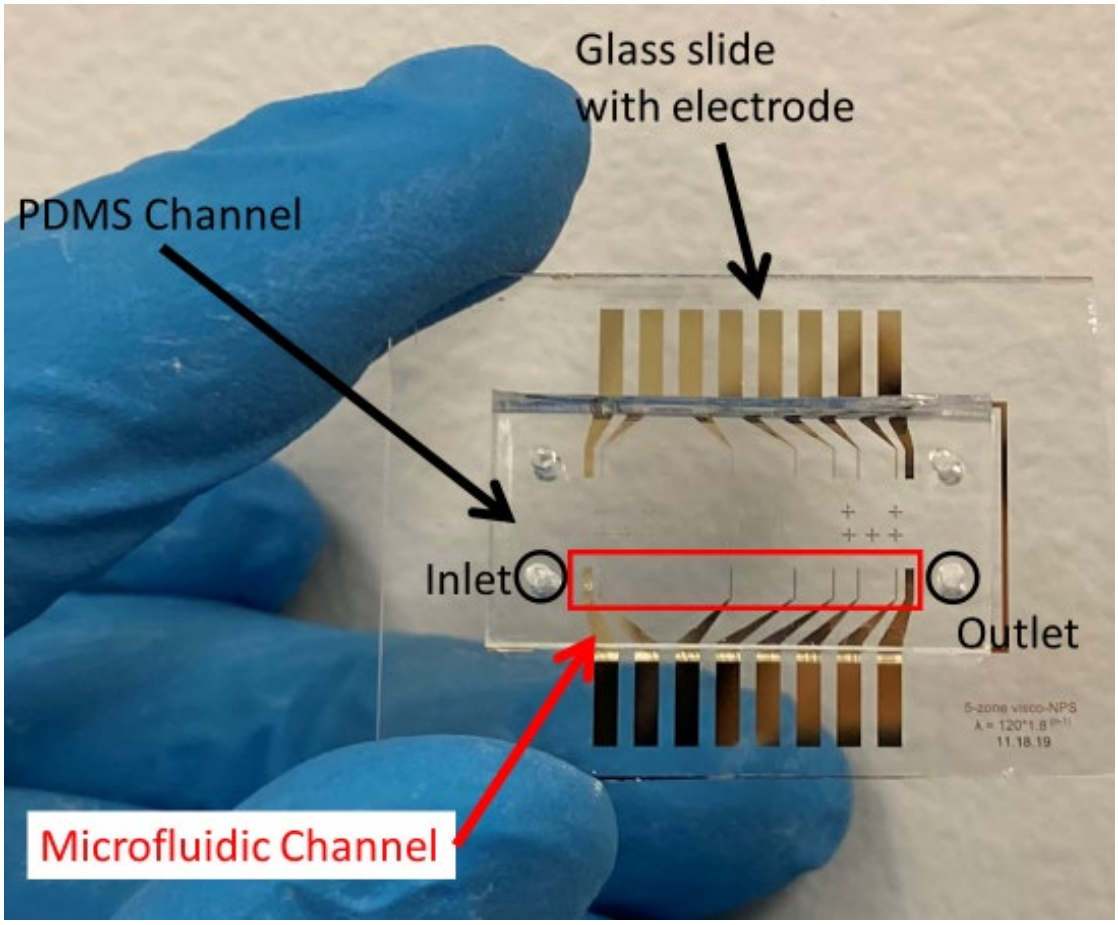

Figure 5-3 Assembled multi-zone viscoNPS device. The PDMS contains the microfluidic channels, while the electrodes are pattered on the glass substrate. These two pieces are irreversibly bonded using oxygen plasma. A cell suspension is loaded into PTFE tubing, which is inserted in the inlet of the microfluidic channel and connected to a microfluidic pump to provide constant pressure-driven flow.

We employed the same lithographic fabrication methods that we used for mz-TEER (described in Section 3.2.2). We created a negative master of the microfluidic channels by first spinning SU8 3025 (MicroChem, Kayaku Advance Materials Inc.) onto a polished silicon wafer at 4000RPM for 30 seconds to achieve a 22 µm thick resist layer. The wafer is baked on a hotplate at 95 ˚C for 10 minutes, and then exposed UV light (272 W, 36 sec) through a photomask. The exposed wafer is subsequently baked on a hot plate at 95 ˚C for 5 minutes and then developed in SU8 developer for 5 minutes. The developed wafer is then cleaned with isopropyl alcohol, dried with nitrogen, and baked for 2 hours at 125 ˚C to prevent cracking of the patterned SU8.

PDMS (SYLGARD 184, Dow Corning Corp.) is mixed at a 10:1 ratio (base: curing agent), poured on top of the wafer with the patterned negative master, and cured at 70 ˚C for two hours. After

curing, the PDMS layer is peeled from the wafer and cut to size. 1.5 mm diameter holes are punched to create inlets and outlets as shown in Figure 5-3.

To pattern electrodes on glass (Fig. 5-4), positive photoresist S1813 (Microchem, Kayaku Advance Materials Inc.) is spun onto a clean glass slide (VWR, USA) at 3000 rpm for 30 seconds to achieve a 1.5 µm thick resist layer. The coated glass slide is baked on a hot plate at 100 ˚C for 1 minute, and then exposed to UV light through a photomask as detailed above for 27 seconds. The slide is then developed by submerging it in MF321 (Microchem, Kayaku Advance Materials Inc.) for 15 seconds, after which deionized (DI) water is used to rinse any residual developer and the slide is dried with nitrogen gas. Electron beam evaporation is used to deposit a 100/250/250 Å layer of Titanium (Ti)/Platinum (Pt)/Gold (Au). Lift-off is performed using acetone to remove excess resist and metal, leaving patterned electrodes on the slide.

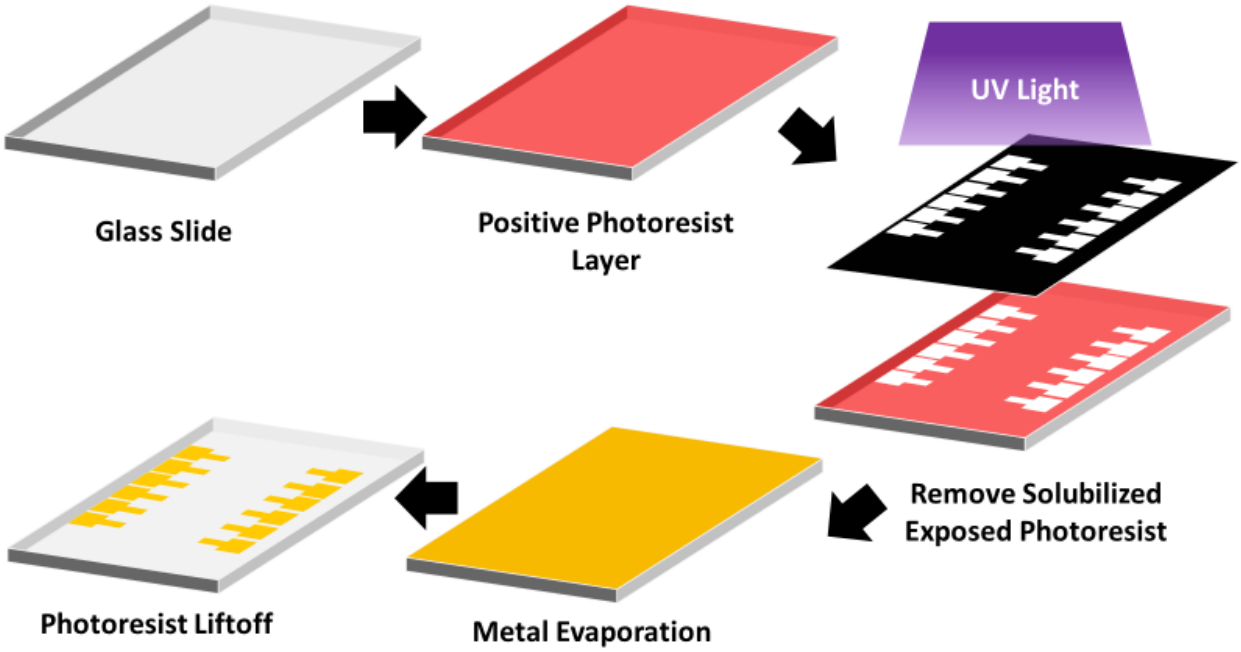

Figure 5-4 Schematic of electrode fabrication protocol using electron beam evaporation. Standard photolithography is used to pattern a positive photoresist on a glass slide. Electron beam evaporation is used to deposit Ti/Pt/Au on the patterned surface of the glass slide. Acetone is employed to lift off polymerized PR, removing with it the excess metal.

To complete the visco-NPS device, the PDMS mold and glass substrate with patterned electrodes are exposed to oxygen plasma (Harrick Plasma, 30 W, 425 mTorr for 1 minute). After exposure, 50 µL of a 2:1 methanol:DI water solution is deposited on top of the glass substate to enable the alignment of the PDMS mold with the patterned electrodes. The devices are baked on a hotplate at 100 ˚C for 1 hour to evaporate the methanol solution and create a permanent bond. An assembled device is presented in Figure 5-3.

5.2.2 Hardware and Software

As discussed in the Introduction, the hardware developed for this platform was modified from the mz-TEER hardware detailed in Chapter 3. The addition of 5 instrumentation amplifiers (INA) enables the circuit to measure from 1 to 6 contraction channels simultaneously. In this platform, the hardware is connected to a USB DAQ (USB-2500, Measurement Computing Corporation) enabling 10 kHz sampling rate and real-time data plotting using a custom MATLAB script (Appendix 8.3).

To accommodate the increase in contact pads due to added electrodes for monitoring each contraction channel, a new pin array was built. This pin array (Figure 5-5B) connects to devices with 1 to 6 total measurement zones (contraction channels). Only a pair of current carrying electrodes (I+ and I-) are used, and the voltage difference is calculated in each of the zones, as described by the table in Figure 5-5. Since the zones are positioned as resistors in series and the applied current along the channel is set by the user, by measuring the voltage drop at each zone, the MATLAB code uses Ohm's Law ($R_{zone} = V_{zone}/I_{total}$) to calculate the resistance in each zone.

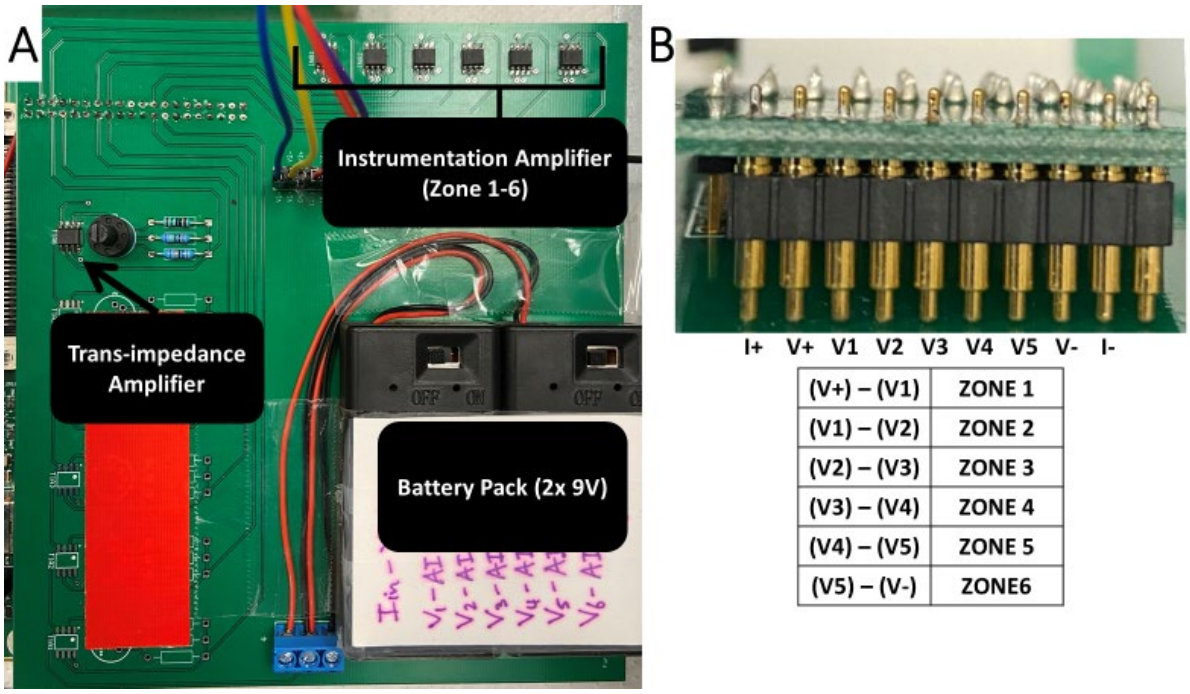

(V+) – (V1)	ZONE 1
(V1) – (V2)	ZONE 2
(V2) – (V3)	ZONE 3
(V3) – (V4)	ZONE 4
(V4) – (V5)	ZONE 5
(V5) – (V-)	ZONE6

Figure 5-5 Custom circuit used to measure individual zones in mz-viscoNPS device. A, Custom circuit containing one trans-impedance amplifier (TIA) that measures the current (I_{total}) through the device and six instrumentation amplifiers (INAs), each of which measures the voltage drop (V_{zone}) across each contraction channel (a maximum of 6). B, Spring-loaded pin array that connects to the electrodes on the glass substrate. The table indicates which voltage measurements are used to calculate the voltage drop (V_{zone}) across each contraction channel (zones 1-6).

5.3 Experimental Methods

In this section, I will discuss the data acquisition process and setup, and the cell suspension preparation used for experiments.

5.3.1 Data acquisition

A MATLAB script (Appendix 8.3) controls the USB-DAQ (USB-2500, Measurement Computing Corporation, USA), which is used to apply a 5 V DC potential across the microfluidic channel. The USB-DAQ also records, at a sample rate of 10 kHz, the voltage drop across each contraction channel. To reduce electronic noise, the USB-DAQ is powered by the battery of a laptop computer, and custom hardware, described in Section 5.2.2, is powered by 9V batteries. This assembly is placed inside a shielded metal box to further reduce electronic noise.

5.3.2 Cell Culture and Preparation

MFC-10A (ATCC CRL-10317) cells were cultured using the Brugge Protocol media recipe. Cells were cultured with DMEM/F12, 5% horse serum, 20ng/mL epidermal growth factor, 0.5mg/mL hydrocortisone, 100ng/mL cholera toxin, 10ug/mL insulin, 1% penicillin-streptomycin and kept in an incubator at 37 ˚C and 5% CO2. Media was changed every 48 hours until cell cultures were 80% confluent. Cells less than Passage 15 were used.

To passage, MCF10-A cells where incubated in 0.25% trypsin/EDTA at 37 ˚C until cells lifted from the culture plate. Growth media was subsequently added (2:1, growth media: trypsin) to neutralize the trypsin, and the cell suspension was centrifuged at 0.5 RCF for 5 minutes then re-suspended at a concentration of 500,000 cells/mL in PBS. This suspension was loaded into a length of PTFE tubing (1.5 mm outer diameter, 0.5 mm inner diameter, Tygon Inc.), which was subsequently connected to the microfluidic device. The tubing was connected to a microfluidic pump (MFCS-EZ, Fluigent Corp.) to drive the cells through the device at a constant pressure.

5.4 Results

In this section, I will present the results of our proof-of-concept platform, mz-viscoNPS, tested with two and four contraction channels. These results confirm the viability of a multi-zone approach and indicate key areas of improvements for the next design iteration.

5.4.1 mz-viscoNPS Viability Testing

We first designed a two-zone microfluidic channel to test the capability of the hardware to make simultaneous measurements. This design includes two zones of equal length (2 mm), the first with four periods and the second with eight periods (Figure 5-6A). Panel B shows the resistance pulse as an MCF-10A cell crosses the first and second contraction channel. To characterize the effect of periodic length on the resistance pulse, we quantified the peak height of each period and calculated the coefficient of variation. Ideally, the sinusoidal response curve should have constant peak height, indicating that the cell deforms in the same way as it moves through each period of the sinusoidal channel. Periodic length (Lp) is defined as:

$$L_{period} = \frac{N_{periods}}{L_{channel}} \tag{2}$$

where $N_{periods}$ corresponds to the number of periods in a contraction channel of length $L_{channel}$. The coefficient of variation of peak height for each zone is plotted in Panel C; Zone 1 (L_p = 500 µm) has five times less variation in peak height than Zone 2 (L_p = 250 µm).

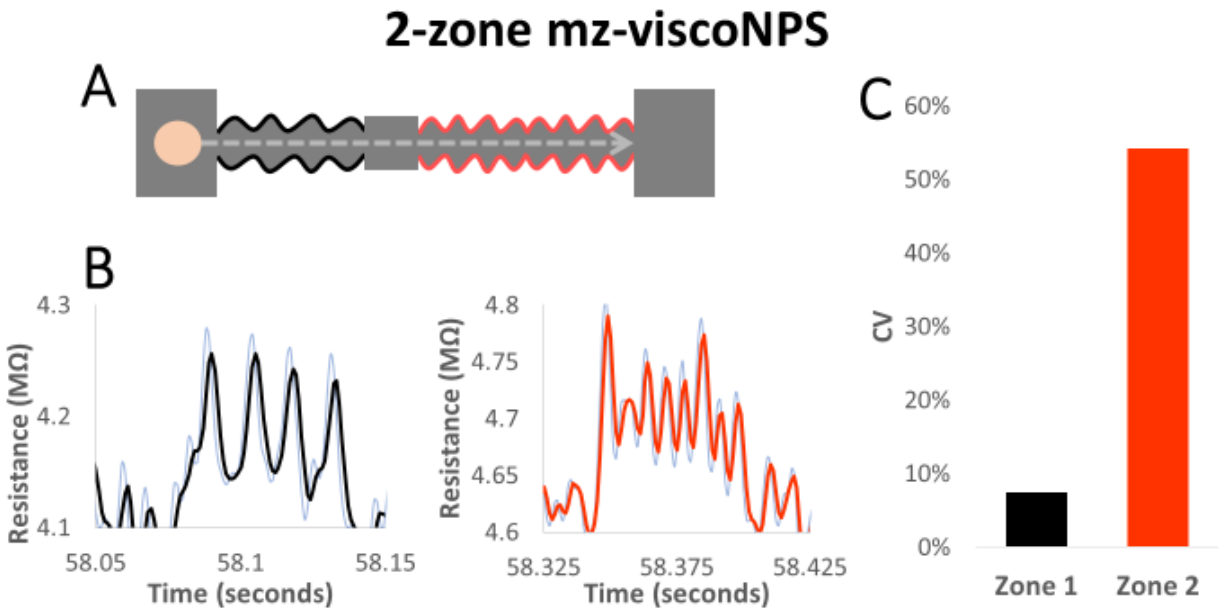

Figure 5-6 Schematic and representative resistance traces for a two-zone mz-viscoNPS measurement as an MCF-10A cell flows through the channel. A, Schematic of sinusoidal contraction channels with length of 2 mm and either four or eight periods. B, Resistance pulse from each channel when an MCF-10A cell passes through (driven at 1 psi), resulting in a measurement frequency of 80 Hz (contraction channel 1) and 160 Hz (contraction channel 2). C, Coefficient of variation of peak height in the response signal indicates greater peak height variability in Zone 2 than Zone 1.

Following the success of our two-zone device, we tested a four-zone device. As in the two-zone device, the length of each of the four contraction channels was 2 mm, with zones 1-4 containing 4, 8, 12, and 16 periods, respectively (Figure 5-7A). Our hardware and software successfully measured four contraction channels simultaneously (Figure 5-7B). The large differences in CV of peak height between contraction channels (Figure 5-7C) highlights the importance of periodic length in our measurements. Together, these data confirm the ability of our proof-of-concept platform to measure up to four contraction channels simultaneously and suggest that the minimum periodic length should be 500 µm. Our hardware is currently limited to six zones by the pin-array (Figure 5-5B). We anticipate that our hardware and software are capable of simultaneously measuring more than six contraction channels by increasing the number of parallel measurement circuits and by using longer, commercially available, pin arrays; further investigation is required to determine the maximum number of simultaneous measurements possible with this platform.

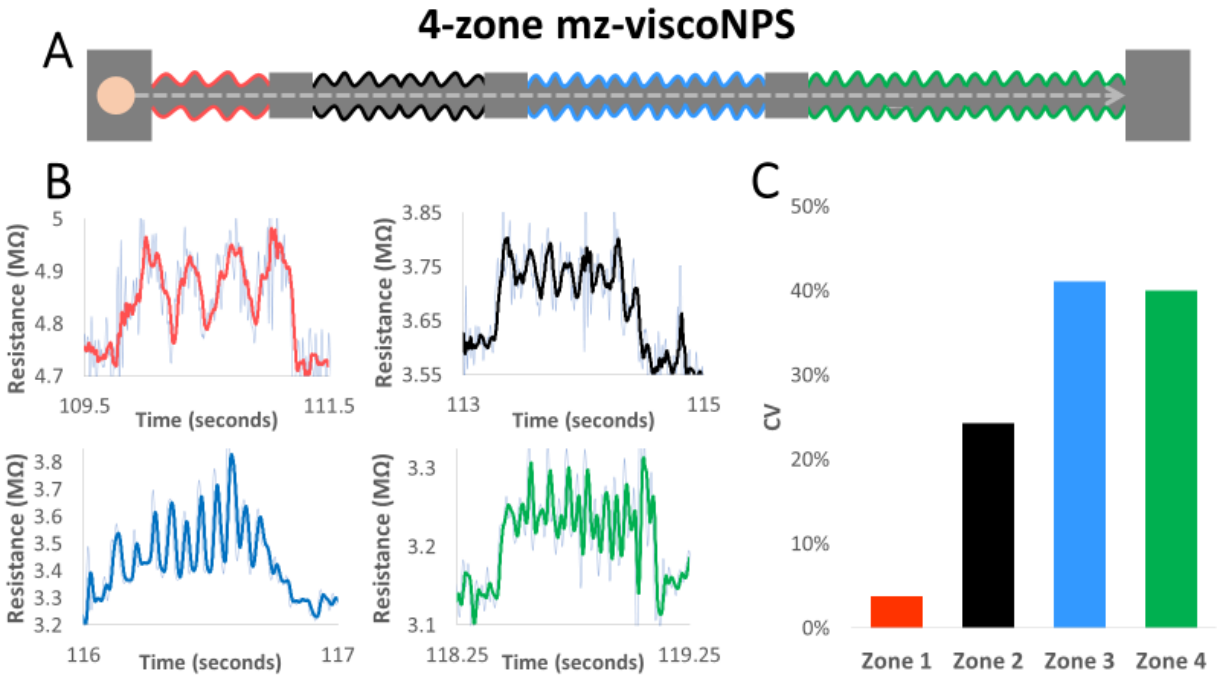

Figure 5-7 Schematic and resistance data for a four-zone mz-viscoNPS device. A, Schematic of sinusoidal contraction channels. The first contraction channel has 4 periods, the second has 8, the third has 12, and the fourth has 16, all with a length of 2 mm. B, Representative resistance pulse from each channel when an MCF-10A cell passes through (driven at 1 psi), resulting in a measurement frequency of 3 Hz (contraction channel 1), 4 Hz (contraction channel 2), 10 Hz (contraction channel 3), and 20 Hz (contraction channel 4). C, Coefficient of variation of peak height in the response signal indicates greater peak height variability in Zones 2, 3, and 4 than Zone 1.

5.5 Discussion

This proof-of-concept mz-viscoNPS platform has yielded key results that will inform the next design iteration. Most importantly, we have demonstrated the ability to simultaneously measure resistance in up to four contraction channels within the same microfluidic channel. The success of this viability test establishes the multi-zone measurement approach as the foundation for the next generation of mz-viscoNPS capable of measuring the viscoelastic properties of single cells at multiple user-defined frequencies. Multi-zone measurements will provide the resolution necessary to investigate the effect on cell viscosity of repeated deformation, were cells are deformed in consecutive contraction channels with matched frequencies. Multi-zone measurements will further allow investigating the impacts of high- and low-frequency deformation on cell structure by deforming cells at different frequencies in rapid succession and independently measuring cell response at each frequency. Regardless of future applications of multi-zone measurements, the data presented in this chapter demonstrates the successful development of hardware and software to measure multiple contraction zones, thus providing a strong foundation for the development of the next-generation multi-zone viscoNPS.

6 CONCLUSIONS AND FUTURE RESEARCH

Chapter Overview

In this chapter, I will summarize the results of the dissertation research and provide conclusions and recommendations for future research using the mz-TEER and mz-viscoNPS platforms based on major fabrication, validation and viability milestones.

6.1 Summary and Findings

In this dissertation, I have presented the integration of a multi-zone approach for electrical resistance measurements to characterize monolayer barrier function and single-cell viscoelastic measurements. The multi-zone TEER measurements device, mz-TEER, is a novel tool that enables investigation of the heterogeneity of cellular monolayers. Furthermore, it permits scientists to expose specific areas of the cell monolayer to chemical cues, and by measuring the effects of these cues on distant zones, it will improve our understanding of how cells communicate along a monolayer (both spatially and temporally). Using the knowledge gained from developing mz-TEER, I also developed new hardware and software that enable multi-zone viscoNPS measurements, allowing viscoelastic measurement of single-cells using 1-4 distinct user-defined frequencies.

In Chapter 4, I described the development of mz-TEER, a microfluidic platform that enables multi-zone trans-endothelial electrical resistance (TEER) measurements. First, I detailed how we designed a two-layer PDMS device combined with a porous membrane that recapitulates the apical and basal chamber of a traditional Transwell Assay, thus enabling TEER measurements. Furthermore, by creating four distinct basal chambers, this first-of-its-kind device permited multiple TEER measurements along the same monolayer, an improvement from traditional bulk measurements. Along with the PDMS device, a custom electrode interface, circuit, and software was developed to accommodate this multi-zone capability. Using this setup, we demonstrated a maximum error of 1.1%, with a measurement every 15 seconds (within each zone). Additionally, our platform was capable of monolayer culture for up to 14 days using MCF-7GFP cells, corroborating the sterilization and cell culture protocols developed. Furthermore, I showed that our platform measured TEER autonomously while the samples were kept inside an incubator, in contrast with TA, where the plates must be taken out of the incubator to perform TEER measurements. At the end of Chapter 4, I demonstrated that mz-TEER is capable of detecting the dissociation (0.25% trypsin exposure) of an MCF-7GFP monolayer, showing a decrease in normalized resistance value over the first 10 minutes, after which it stabilized to baseline. Altogether, my results show that mz-TEER was capable of measuring four distinct zones within a monolayer, and could detect monolayer dissociation.

In Chapter 5, I introduced a proof-of-concept platform in which I aimed to integrate a multi-zone approach to a platform developed in the Sohn Lab, viscoNPS, that measures single cell viscoelastic properties. viscoNPS works by flowing single cells through a sinusoidal contraction channel, inducing periodic deformation which allows for the extraction storage (G'', elasticity) and loss (G', viscosity) modulus. I used knowledge from developing the mz-TEER platform to integrate up to

four contraction channels, each with a different user-defined frequency. I used MCF10-A cells to test devices with two or four zones, successfully detecting cells traversing each of the contraction channels. Furthermore, quantification of peak height in the response signal suggested further investigation about the geometric design of the channels is needed to ensure cells deform reproducibly while traversing the contraction channels. Together, these results serve as a blueprint for the development of the next generation mz-viscoNPS.

6.2 Future Work

In this dissertation, I have presented the development of two novel platforms: one that improves the spatial and temporal resolution of TEER measurements, and another which enables the viscoelastic measurements of single-cells at various frequencies.

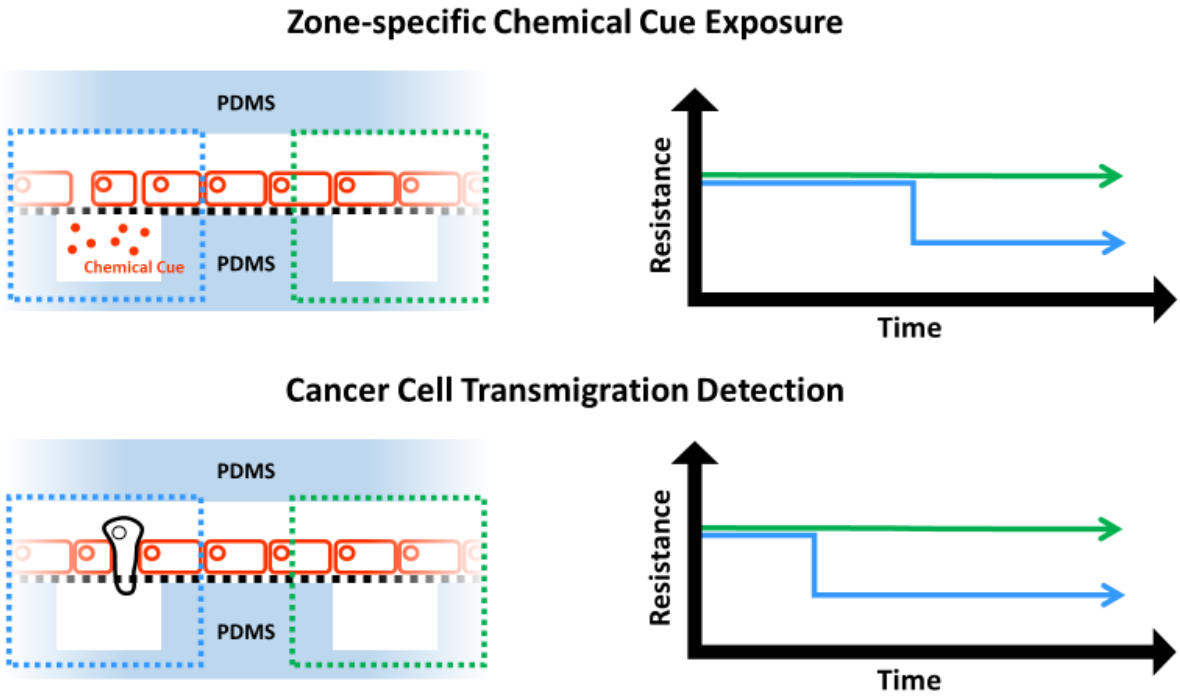

Figure 6-1 mz-TEER future work schematics. Top: Schematic showing the zone-specific effects of chemical cues introduced through the basal channel. These effects will be quantified using TEER with effects detected in unexposed zones elucidating of spatial and temporal extent of the exposure. Bottom: Schematic of mz-TEER detecting cancer cell transmigration. A cell migrates across the monolayer through cell-cell junctions inducing a drop in the zone's resistance.

In relation to the mz-TEER device, the discussed results validate the protocols developed for monolayer culture and TEER measurements. Future work should include experiments regarding the effect of zone-specific exposure to chemical cues (e.g. TNF-α), where a zone is exposed through its basal channel, while the other three zones remain unexposed (Fig. 6-1). By monitoring TEER changes on the unexposed zones, we can improve our understanding of the spatial and temporal effects of any chosen selected cues. Regarding metastasis, the mz-TEER platform is

designed to detect cancer cell transmigration across the monolayer. For this experiment, cancer cells are introduced into the apical channel once the monolayer has reached complete confluency. TEER is monitored in all zones while cancer cells transmigrate across the monolayer to the basal channel, and since during this process migrating cells create a pore at the cell-cell junctions, a drop in TEER should be detected. Furthermore, to increase spatial resolution, smaller zones should be tested (e.g. 500um x 1mm, 250um x 1mm), resulting in designs with more than four measurement zones.

For the multi-zone viscoNPS, which is already in use in the Sohn Lab, further investigation on the amount of contraction channel is needed to understand the effects of consecutive deformation on single cells. Does the measurement in the first contraction channel affect the following measurements? To test this, cells are flowed through a mz-viscoNPS with, for example, four identical contraction channels and the resistance pulse for each contraction should match. Differences in the pulse would indicate that previous deformation does have an effect in our measurements. To alleviate this, the contraction channels should be placed farther apart, allowing the cell to relax between measurements. Furthermore, by investigating which frequencies best capture changes in the cells' cytoskeleton, nucleus, and membrane, the contraction channels can be tuned to detect specific cellular processes (e.g. cell cycle, malignant progression).

Throughout this dissertation, I have detailed the development of two microfluidic platforms that use a multi-zone resistance measurement approach to improve the spatial and temporal resolution of TEER measurements, and to advance single-cell viscoelastic measurements using viscoNPS.

7 BIBLIOGRAPHY

1. Carbonaro a, Sohn LL. A resistive-pulse sensor chip for multianalyte immunoassays. *Lab Chip*. 2005;5(10):1155-1160. doi:10.1039/b504827c
2. Balakrishnan KR, Whang JC, Hwang R, Hack JH, Lucy A, Sohn LL. Node-Pore Sensing Enables Label-Free Surface-Marker Profiling of Single Cells Supporting Information Table of Contents. :1-15.
3. Carbonaro A, Mohanty SK, Huang H, Godley L a, Sohn LL. Cell characterization using a protein-functionalized pore. *Lab Chip*. 2008;8(9):1478-1485. doi:10.1039/b801929k
4. Hughes AJ, Spelke DP, Xu Z, Kang C-C, Schaffer D V, Herr AE. Single-cell western blotting. *Nat Methods*. 2014;11(7):749-755. doi:10.1038/nmeth.2992
5. Hou HW, Li QS, Lee GYH, Kumar AP, Ong CN, Lim CT. Deformability study of breast cancer cells using microfluidics. *Biomed Microdevices*. 2009;11(3):557-564. doi:10.1007/s10544-008-9262-8
6. Lecault V, White AK, Singhal A, Hansen CL. Microfluidic single cell analysis: From promise to practice. *Curr Opin Chem Biol*. 2012;16(3-4):381-390. doi:10.1016/j.cbpa.2012.03.022
7. Falcón-banchs R, Rivest F, Sohn LL. Single-cell Label-free Profiling RS PA RS. 2017:1-18. doi:10.1002/9780470027318.a9565
8. Darling EM, Di Carlo D. *High-Throughput Assessment of Cellular Mechanical Properties*. Vol 17.; 2015. doi:10.1146/annurev-bioeng-071114-040545
9. Centers for Disease Control and Prevention. An Update on Cancer Deaths in the United States. 2020. https://www.cdc.gov/cancer/dcpc/research/update-on-cancer-deaths/index.htm. Published 2020.
10. Li QS, Lee GYH, Ong CN, Lim CT. AFM indentation study of breast cancer cells. *Biochem Biophys Res Commun*. 2008;374(4):609-613. doi:10.1016/j.bbrc.2008.07.078
11. Zervantonakis IK, Hughes-Alford SK, Charest JL, Condeelis JS, Gertler FB, Kamm RD. Three-dimensional microfluidic model for tumor cell intravasation and endothelial barrier function. *Proc Natl Acad Sci*. 2012;109(34):13515-13520. doi:10.1073/pnas.1210182109
12. Lehman HL, Dashner EJ, Lucey M, et al. Modeling and characterization of inflammatory breast cancer emboli grown in vitro. *Int J Cancer*. 2013;132(10):2283-2294. doi:10.1002/ijc.27928
13. Mierke CT. The fundamental role of mechanical properties in the progression of cancer disease and inflammation. *Reports Prog Phys*. 2014;77(7):076602. doi:10.1088/0034-4885/77/7/076602
14. Kozminsky M, Sohn LL. The promise of single-cell mechanophenotyping for clinical applications. *Biomicrofluidics*. 2020;14(3). doi:10.1063/5.0010800
15. Coghlin C, Murray GI. Current and emerging concepts in tumour metastasis. *J Pathol*. 2010;222(1):1-15. doi:10.1002/path.2727
16. Reymond N, D'Água BB, Ridley AJ. Crossing the endothelial barrier during metastasis. *Nat Rev Cancer*. 2013;13(12):858-870. doi:10.1038/nrc3628
17. Hou HW, Bhagat AAS, Lin Chong AG, et al. Deformability based cell margination—A simple microfluidic design for malaria-infected erythrocyte separation. *Lab Chip*. 2010;10(19):2605. doi:10.1039/c003873c
18. Woodfin A, Voisin M-B, Beyrau M, et al. The junctional adhesion molecule JAM-C

regulates polarized transendothelial migration of neutrophils in vivo. *Nat Immunol*. 2011;12(8):761-769. doi:10.1038/ni.2062
19. Katt ME, Placone AL, Wong AD, Xu ZS, Searson PC. In Vitro Tumor Models: Advantages, Disadvantages, Variables, and Selecting the Right Platform. *Front Bioeng Biotechnol*. 2016;4(February):12. doi:10.3389/fbioe.2016.00012
20. Furie MB, Cramer EB, Naprstek BL, Silverstein SC. Cultured endothelial cell monolayers that restrict the transendothelial passage of macromolecules and electrical current. *J Cell Biol*. 1984;98(3):1033-1041. doi:10.1083/jcb.98.3.1033
21. Shulman Z, Alon R. Chapter 14 Real-Time In Vitro Assays For Studying the Role of Chemokines in Lymphocyte Transendothelial Migration Under Physiologic Flow Conditions. *Methods Enzymol*. 2009;461(B):311-332. doi:10.1016/S0076-6879(09)05414-7
22. Vogel PA, Halpin ST, Martin RS, Spence DM. Microfluidic transendothelial electrical resistance measurement device that enables blood flow and postgrowth experiments. *Anal Chem*. 2011;83(11):4296-4301. doi:10.1021/ac2004746
23. Wang X-Y, Jin Z-H, Gan B-W, Lv S-W, Xie M, Huang W-H. Engineering interconnected 3D vascular networks in hydrogels using molded sodium alginate lattice as the sacrificial template. *Lab Chip*. 2014;14(15):2709-2716. doi:10.1039/c4lc00069b
24. Srinivasan B, Kolli AR, Esch MB, Abaci HE, Shuler ML, Hickman JJ. TEER Measurement Techniques for In Vitro Barrier Model Systems. *J Lab Autom*. 2015;20(2):107-126. doi:10.1177/2211068214561025
25. Mermoud Y, Felder M, Stucki JD, Stucki AO, Guenat OT. Microimpedance tomography system to monitor cell activity and membrane movements in a breathing lung-on-chip. *Sensors Actuators, B Chem*. 2018;255:3647-3653. doi:10.1016/j.snb.2017.09.192
26. Ferrell N, Desai RR, Fleischman AJ, Roy S, Humes HD, Fissell WH. A microfluidic bioreactor with integrated transepithelial electrical resistance (TEER) measurement electrodes for evaluation of renal epithelial cells. *Biotechnol Bioeng*. 2010;107(4):707-716. doi:10.1002/bit.22835
27. Kim Y, Lobatto ME, Kawahara T, et al. Probing nanoparticle translocation across the permeable endothelium in experimental atherosclerosis. *Proc Natl Acad Sci U S A*. 2014;111(3):1078-1083. doi:10.1073/pnas.1322725111
28. Yeste J, Illa X, Gutiérrez C, Solé M, Guimerà A, Villa R. Geometric correction factor for transepithelial electrical resistance measurements in transwell and microfluidic cell cultures. *J Phys D Appl Phys*. 2016;49(37). doi:10.1088/0022-3727/49/37/375401
29. Kim J, Li B, Scheideler OJ, Kim Y, Sohn LL. Visco-Node-Pore Sensing: A Microfluidic Rheology Platform to Characterize Viscoelastic Properties of Epithelial Cells. *iScience*. 2019;13:214-228. doi:10.1016/j.isci.2019.02.021
30. Parks JE. ` Ohm ' s Law III -- Resistors in Series and Parallel. *Dep Phys Astron 401 Nielsen Phys Build Univ Tennessee Knoxville, Tennessee 37996-1200*. 2007:1-18.
31. Blythe AR. Electrical resistivity measurements of polymer materials. *Polym Test*. 1984;4(2-4):195-209. doi:10.1016/0142-9418(84)90012-6
32. SINGH Y. Electrical Resistivity Measurements: a Review. *Int J Mod Phys Conf Ser*. 2013;22:745-756. doi:10.1142/s2010194513010970
33. Saleh OA, Sohn LL. Quantitative sensing of nanoscale colloids using a microchip Coulter counter. *Rev Sci Instrum*. 2001;72(12):4449. doi:10.1063/1.1419224
34. Saleh OA, Sohn LL. Quantitative sensing of nanoscale colloids using a microchip Coulter

counter. *Rev Sci Instrum*. 2001;72(12):4449-4451. doi:10.1063/1.1419224
35. Li X, Li H, Liu C, et al. CLDN6-mediates SB431542 action through MMPs to regulate the invasion, migration, and EMT of breast cancer cells. *Int J Clin Exp Pathol*. 2020;13(7):1590-1600.
36. Henry OYF, Villenave R, Cronce MJ, Leineweber WD, Benz MA, Ingber DE. Organs-on-chips with integrated electrodes for trans-epithelial electrical resistance (TEER) measurements of human epithelial barrier function. *Lab Chip*. 2017;17(13):2264-2271. doi:10.1039/c7lc00155j
37. Vu K, Weksler B, Romero I, Couraud PO, Gelli A. Immortalized human brain endothelial cell line HCMEC/D3 as a model of the blood-brain barrier facilitates in vitro studies of central nervous system infection by cryptococcus neoformans. *Eukaryot Cell*. 2009;8(11):1803-1807. doi:10.1128/EC.00240-09
38. Maoz BM, Herland A, Henry OYF, et al. Organs-on-Chips with combined multi-electrode array and transepithelial electrical resistance measurement capabilities. *Lab Chip*. 2017;17(13):2294-2302. doi:10.1039/c7lc00412e
39. Booth R, Kim H. Characterization of a microfluidic in vitro model of the blood-brain barrier (μBBB). *Lab Chip*. 2012;12(10):1784. doi:10.1039/c2lc40094d
40. Al-Azzawi S, Masheta D, Guildford AL, Phillips G, Santin M. Dendrimeric poly(Epsilon-lysine) delivery systems for the enhanced permeability of flurbiprofen across the blood-brain barrier in Alzheimer's disease. *Int J Mol Sci*. 2018;19(10):1-18. doi:10.3390/ijms19103224
41. Kim Y, Lobatto ME, Kawahara T, et al. Probing nanoparticle translocation across the permeable endothelium in experimental atherosclerosis. *Proc Natl Acad Sci U S A*. 2014;111(3):1078-1083. doi:10.1073/pnas.1322725111
42. Odijk M, Van Der Meer AD, Levner D, et al. Measuring direct current trans-epithelial electrical resistance in organ-on-a-chip microsystems. *Lab Chip*. 2015;15(3):745-752. doi:10.1039/c4lc01219d
43. Sohn LL, Saleh O a, Facer GR, Beavis a J, Allan RS, Notterman D a. Capacitance cytometry: measuring biological cells one by one. *Proc Natl Acad Sci U S A*. 2000;97(20):10687-10690. doi:10.1073/pnas.200361297
44. Kim J, Han S, Lei A, et al. Characterizing cellular mechanical phenotypes with mechano-node-pore sensing. *Microsystems Nanoeng*. 2018;4(1):1-12. doi:10.1038/micronano.2017.91
45. Hong J, Kandasamy K, Marimuthu M, Choi CS, Kim S. Electrical cell-substrate impedance sensing as a non-invasive tool for cancer cell study. *Analyst*. 2011;136(2):237-245. doi:10.1039/C0AN00560F
46. Rönkkö S, Vellonen K-S, Järvinen K, Toropainen E, Urtti A. Human corneal cell culture models for drug toxicity studies. *Drug Deliv Transl Res*. 2016. doi:10.1007/s13346-016-0330-y
47. Santander J, Fonseca L, Udina S, Marco S. Real-Time Physiological Sensors Based Liver-on-Chip Device for Monitoring Drug Toxicity. *J Micromechanics Microengineering Accept*. 2007. doi:10.1016/j.snb.2007.07.003
48. Bhatia SN, Ingber DE. Microfluidic organs-on-chips. *Nat Biotechnol*. 2014;32(8):760-772. doi:10.1038/nbt.2989
49. Mazzoleni AP, Sisken BF, Kahler RL. Conductivity values of tissue culture medium from 20°C to 40°C. *Bioelectromagnetics*. 1986;7(1):95-99. doi:10.1002/bem.2250070111

50. Fuhr G, Glasser H, Müller T, Schnelle T. Cell manipulation and cultivation under a.c. electric field influence in highly conductive culture media. *BBA - Gen Subj*. 1994;1201(3):353-360. doi:10.1016/0304-4165(94)90062-0
51. Gitter AH, Bertog M, Schulzke JD, Fromm M. Measurement of paracellular epithelial conductivity by conductance scanning. *Pflugers Arch Eur J Physiol*. 1997;434(6):830-840. doi:10.1007/s004240050472
52. Samy KE, Levy ES, Phong K, Demaree B, Abate AR, Desai TA. Human intestinal spheroids cultured using Sacrificial Micromolding as a model system for studying drug transport. *Sci Rep*. 2019;9(1):1-12. doi:10.1038/s41598-019-46408-0
53. Hur SC, Henderson-MacLennan NK, McCabe ERB, Di Carlo D. Deformability-based cell classification and enrichment using inertial microfluidics. *Lab Chip*. 2011;11(5):912-920. doi:10.1039/c0lc00595a
54. Tanaka M, Bateman R, Rauh D, et al. An unbiased cell morphology-based screen for new, biologically active small molecules. *PLoS Biol*. 2005;3(5):0764-0776. doi:10.1371/journal.pbio.0030128
55. Caille N, Thoumine O, Tardy Y, Meister JJ. Contribution of the nucleus to the mechanical properties of endothelial cells. *J Biomech*. 2002;35(2):177-187. doi:10.1016/S0021-9290(01)00201-9
56. Fabry B, Maksym GN, Hubmayr RD, Butler JP, Fredberg JJ. Implications of heterogeneous bead behavior on cell mechanical properties measured with magnetic twisting cytometry. *J Magn Magn Mater*. 1999;194(1):120-125. doi:10.1016/S0304-8853(98)00564-2
57. Alenghat FJ, Fabry B, Tsai KY, Goldmann WH, Ingber DE. Analysis of cell mechanics in single vinculin-deficient cells using a magnetic tweezer. *Biochem Biophys Res Commun*. 2000;277(1):93-99. doi:10.1006/bbrc.2000.3636
58. Tee SY, Fu J, Chen CS, Janmey PA. Cell shape and substrate rigidity both regulate cell stiffness. *Biophys J*. 2011;100(5):L25-L27. doi:10.1016/j.bpj.2010.12.3744
59. Lulevich V, Zink T, Chen H, Liu F, Liu G. Cell mechanics using atomic force microscopy-based single-cell compression. *Langmuir*. 2006;22(19):8151-8155. doi:10.1021/la060561p
60. Peloquin J, Huynh J, Williams RM, Reinhart-King CA. Indentation measurements of the subendothelial matrix in bovine carotid arteries. *J Biomech*. 2011;44(5):815-821. doi:10.1016/j.jbiomech.2010.12.018
61. Tsai MA, Frank RS, Waugh RE. Passive mechanical behavior of human neutrophils: power-law fluid. *Biophys J*. 1993;65(5):2078-2088. doi:10.1016/S0006-3495(93)81238-4
62. Sato M, Levesque MJ, Nerem RM. Micropipette aspiration of cultured bovine aortic endothelial cells exposed to shear stress. *Arteriosclerosis*. 2015;7(3):276-286. doi:10.1161/01.ATV.7.3.276
63. Kirmizis D, Logothetidis S. Atomic force microscopy probing in the measurement of cell mechanics. *Int J Nanomedicine*. 2010;5(APRIL 2010):137-145. doi:10.2147/IJN.S5787

8 APPENDICES

8.1 Appendix A: PCB Circuit for mzTEER

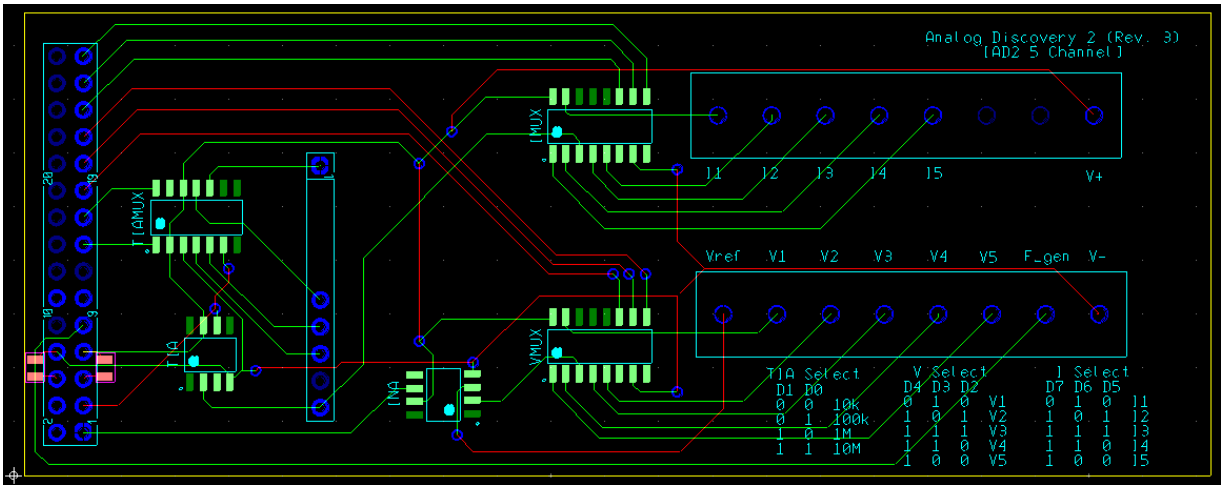

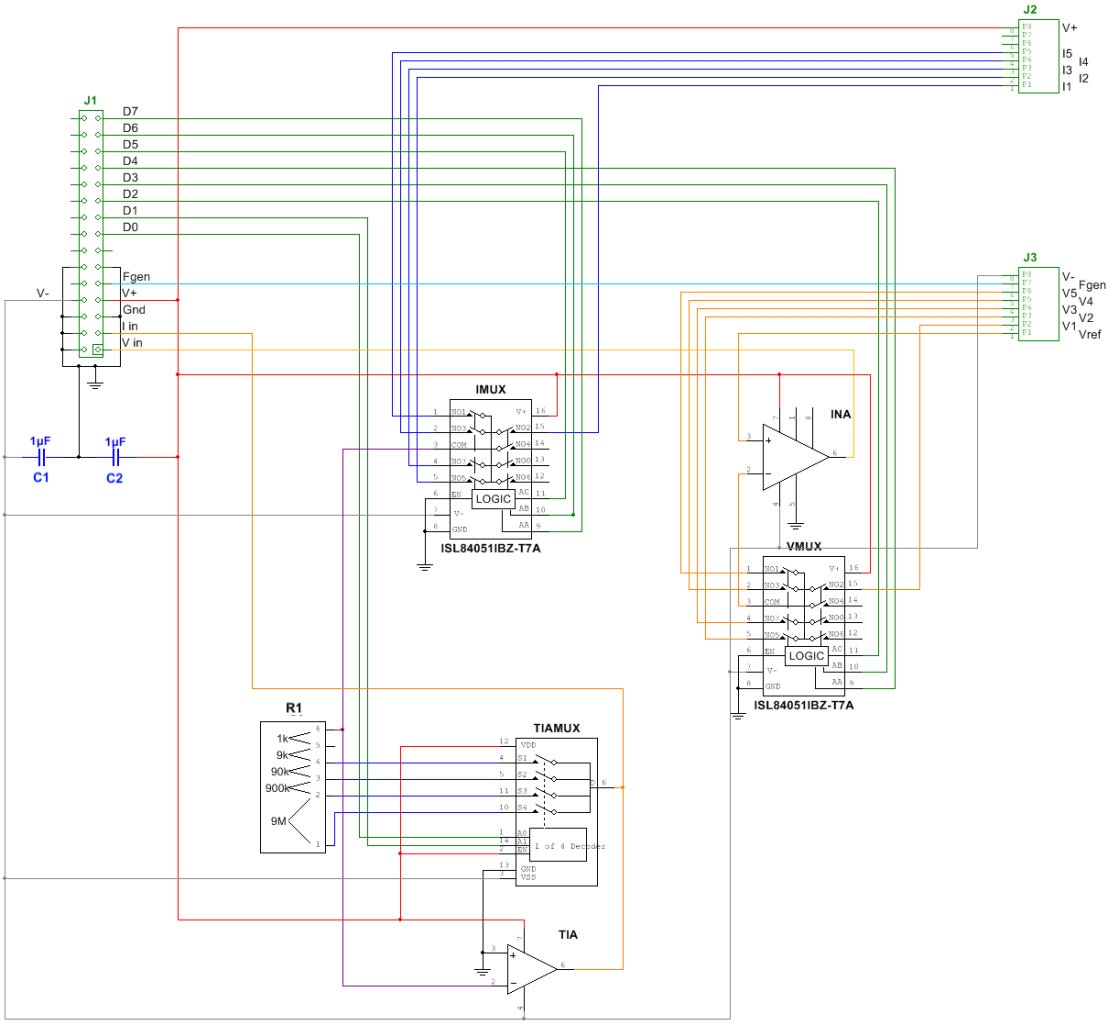

8.2 Appendix B: Python Code for mz-TEER Measurements

```
from ctypes import *
from dwfconstants import *
import math
import time
import matplotlib.pyplot as plt
import sys
import numpy as np
import scipy.signal as sps
from datetime import datetime
from scipy.io import savemat

if sys.platform.startswith("win"):
    dwf = cdll.dwf
elif sys.platform.startswith("darwin"):
    dwf = cdll.LoadLibrary("/Library/Frameworks/dwf.framework/dwf")
else:
    dwf = cdll.LoadLibrary("libdwf.so")

########################################## PARAMS
##################################################
fs = 1e5  # sampling rate [samp/s]
duration = 1  # time to measure each zone [s]
fc = 12  # frequency of stimulus/carrier signal [Hz]
Ac = 0.01  # amplitude of stimulus/carrier signal [V]
numCycles = 120  # number of times to repeat measuring all zones
RTIA = 10e3  # gain resistor of TIA [Ohm]
plotting = False
################################################################################
################
filename = input("Input filename: ")
filepath = "C:/Users/Roberto/Desktop/TEER Python/"+filename+".mat"

now = datetime.now()
current_time = now.strftime("%H:%M:%S")
startTime = current_time
timeStamps = []

impedanceData = np.zeros((numCycles, 5))

# loop over cycles
for cycleNum in range(numCycles):

    print('Cycle', cycleNum)
    if cycleNum > 0:
```

```
    print('Inside waiting')
    #time.sleep(30-15)

# loop over 5 zones
for zoneNum in range(5):
    pinValues = np.zeros(8)
    if RTIA == 10e3:
        pinValues[0:1+1] = np.array([0, 0])
    elif RTIA == 100e3:
        pinValues[0:1+1] = np.array([1, 0])
    elif RTIA == 1e6:
        pinValues[0:1+1] = np.array([0, 1])
    elif RTIA == 10e6:
        pinValues[0:1+1] = np.array([1, 1])
    else:
        print("INVALID RTIA VALUE!!")
    if zoneNum == 0:
        pinValues[2:4+1] = np.array([0, 1, 0])
        pinValues[5:7+1] = np.array([0, 1, 0])
    elif zoneNum == 1:
        pinValues[2:4+1] = np.array([1, 0, 1])
        pinValues[5:7+1] = np.array([1, 0, 1])
    elif zoneNum == 2:
        pinValues[2:4+1] = np.array([1, 1, 1])
        pinValues[5:7+1] = np.array([1, 1, 1])
    elif zoneNum == 3:
        pinValues[2:4+1] = np.array([0, 1, 1])
        pinValues[5:7+1] = np.array([0, 1, 1])
    elif zoneNum == 4:
        pinValues[2:4+1] = np.array([0, 0, 1])
        pinValues[5:7+1] = np.array([0, 0, 1])

    # declare ctype variables
    hdwf = c_int()
    sts = c_byte()
    hzAcq = c_double(fs)
    nSamples = int(duration * fs)  # [samples]
    vSamples = (c_double*nSamples)()
    iSamples = (c_double*nSamples)()
    cAvailable = c_int()
    cLost = c_int()
    cCorrupted = c_int()
    fLost = 0
    fCorrupted = 0

    # print(DWF version)
```

```
    version = create_string_buffer(16)
    dwf.FDwfGetVersion(version)
    # print("DWF Version: "+str(version.value))

    # open device
    # print("Opening first device")
    dwf.FDwfDeviceOpen(c_int(-1), byref(hdwf))

    if hdwf.value == hdwfNone.value:
        szerr = create_string_buffer(512)
        dwf.FDwfGetLastErrorMsg(szerr)
        print(str(szerr.value))
        print("failed to open device")
        quit()

    # set up analog IO channel nodes (voltage supplies)
    dwf.FDwfAnalogIOChannelNodeSet(hdwf, c_int(0), c_int(0), c_double(True))  # enable
positive supply
    dwf.FDwfAnalogIOChannelNodeSet(hdwf, c_int(0), c_int(1), c_double(5.0))  # set voltage
to 5 V
    dwf.FDwfAnalogIOChannelNodeSet(hdwf, c_int(1), c_int(0), c_double(True))  # enable
negative supply
    dwf.FDwfAnalogIOChannelNodeSet(hdwf, c_int(1), c_int(1), c_double(-5.0))  # set voltage
to -5 V
    dwf.FDwfAnalogIOEnableSet(hdwf, c_int(True))  # master enable

################################################################################
##################################
    # set gain muxes and data mux
    # print("Setting digital pins...")
    hzSys = c_double()
    dwf.FDwfDigitalOutInternalClockInfo(hdwf, byref(hzSys))
    for pinNum in range(len(pinValues)):
        dwf.FDwfDigitalOutEnableSet(hdwf, c_int(pinNum), c_int(1))  # enable pin
        dwf.FDwfDigitalOutDividerSet(hdwf, c_int(pinNum), c_int(int(hzSys.value)))
        if pinValues[pinNum] == 0:
            dwf.FDwfDigitalOutCounterSet(hdwf, c_int(pinNum), c_int(1), c_int(0))  # 1 tick low,
0 tick high
        elif pinValues[pinNum] == 1:
            dwf.FDwfDigitalOutCounterSet(hdwf, c_int(pinNum), c_int(0), c_int(1))  # 0 tick low,
1 tick high
    dwf.FDwfDigitalOutConFigure(hdwf, c_int(1))  # master enable?
    # print("Digital pins set!")

################################################################################
##################################
```

```
        # print("Generating sine wave...")
        dwf.FDwfAnalogOutNodeEnableSet(hdwf, c_int(0), AnalogOutNodeCarrier, c_bool(True))
        dwf.FDwfAnalogOutNodeFunctionSet(hdwf, c_int(0), AnalogOutNodeCarrier, funcSine)
        dwf.FDwfAnalogOutNodeFrequencySet(hdwf, c_int(0), AnalogOutNodeCarrier,
c_double(fc))
        dwf.FDwfAnalogOutNodeAmplitudeSet(hdwf, c_int(0), AnalogOutNodeCarrier,
c_double(Ac))
        dwf.FDwfAnalogOutConFigure(hdwf, c_int(0), c_bool(True))

        # set up acquisition
        dwf.FDwfAnalogInChannelEnableSet(hdwf, c_int(0), c_bool(True))
        dwf.FDwfAnalogInChannelEnableSet(hdwf, c_int(1), c_bool(True))
        dwf.FDwfAnalogInChannelRangeSet(hdwf, c_int(0), c_double(5.0))
        dwf.FDwfAnalogInChannelRangeSet(hdwf, c_int(1), c_double(5.0))
        dwf.FDwfAnalogInAcquisitionModeSet(hdwf, acqmodeRecord)
        dwf.FDwfAnalogInFrequencySet(hdwf, c_double(fs))
        dwf.FDwfAnalogInRecordLengthSet(hdwf, c_double(duration))  # -1 infinite record length

        # wait at least 2 seconds for the offset to stabilize
        time.sleep(2.0)

        # print("Starting oscilloscopes")
        dwf.FDwfAnalogInConFigure(hdwf, c_int(0), c_int(1))  # master enable for analog in?

        cSamples = 0
        now = datetime.now()
        current_time = now.strftime("%H:%M:%S")
        timeStamps.append(current_time)

        print(f"Starting acquisition: cycle #{cycleNum+1}, zone #{zoneNum+1}")
        # it = 0
        while cSamples < nSamples:
            # it = it + 1
            # print("iter "+str(it))
            dwf.FDwfAnalogInStatus(hdwf, c_int(1), byref(sts))
            if cSamples == 0 and (sts == DwfStateConfig or sts == DwfStatePrefill or sts ==
DwfStateArmed):
                # Acquisition not yet started.
                continue

            dwf.FDwfAnalogInStatusRecord(hdwf, byref(cAvailable), byref(cLost),
byref(cCorrupted))

            cSamples += cLost.value

            if cLost.value:
```

```
            fLost = 1
        if cCorrupted.value:
            fCorrupted = 1

        if cAvailable.value == 0:
            continue

        if cSamples+cAvailable.value > nSamples:
            cAvailable = c_int(nSamples-cSamples)

        # get channel 1 data
        dwf.FDwfAnalogInStatusData(hdwf, c_int(0), byref(vSamples,
sizeof(c_double)*cSamples), cAvailable)
        # get channel 2 data
        dwf.FDwfAnalogInStatusData(hdwf, c_int(1), byref(iSamples,          cSamples +=
cAvailable.value
        # print("cSamples = "+str(cSamples))

    dwf.FDwfAnalogOutReset(hdwf, c_int(0))
    dwf.FDwfDigitalOutReset(hdwf)
    dwf.FDwfDeviceCloseAll()

    # print("Recording done")
    if fLost:
        print("Samples were lost! Reduce frequency")
    if fCorrupted:
        print("Samples could be corrupted! Reduce frequency")

    V = np.fromiter(vSamples, dtype=np.float)
    I = np.fromiter(iSamples, dtype=np.float) / -RTIA
    t = np.arange(0, nSamples) / fs

    # remove DC offsets...
    V_m = np.mean(V)
    I_m = np.mean(I)
    V = V - V_m
    I = I - I_m
    # print("Means: ",V_m, I_m*RTIA)

    # IQ demodulation
    mixI = 2*np.cos(2*np.pi*fc*t)
    mixQ = -2*np.sin(2*np.pi*fc*t)
    V_IQ = V * mixI + 1j * V * mixQ
    I_IQ = I * mixI + 1j * I * mixQ

##########################################################################################
```

```
##################
        # get the mean resistance value
        V_mean = np.mean(V_IQ)
        I_mean = np.mean(I_IQ)
        Z_mean = V_mean / I_mean
        R_mean = np.abs(Z_mean)
        print(f'Resistance = {np.round(R_mean/1e3, 3)} kOhms @
{np.round(np.angle(Z_mean)/np.pi*180, 3)} deg")
        impedanceData[cycleNum, zoneNum] = R_mean

#############################################################################################
##################
        if plotting:
            plt.Figure()
            mask = t < 5. / 12.
            plt.plot(t[mask], V[mask])
            plt.plot(t[mask], I[mask] * -RTIA)
            plt.legend(["IN1", "IN2"])
            plt.ylabel("Voltage [V]")
            plt.xlabel("Time [s]")
            plt.title(f"Cycle #{cycleNum+1}, Zone #{zoneNum+1}")
            plt.show()

now = datetime.now()
current_time = now.strftime("%H:%M:%S")
endTime = current_time

# save data
mdict = {"startTime": startTime, "endTime": endTime, "impedanceData": impedanceData,
"RTIA": RTIA, "sampRate": fs, "freqVin": fc, "Vpeak": Ac, "timeStamps": timeStamps}
savemat(filepath, mdict)
```

8.3 Appendix C: MATLAB Code for mz-viscoNPS

```
%% NPS acquisition script for MCC DAQ
% Alan Dong
% edits: Roberto Falcon
% 2019-03-08

%% stop and release previous session if needed
if exist('s', 'var')
   stop(s);
   release(s);
end
fclose all;
close all;
clear;

%% ACQUISITION PARAMETERS
sampleRate = 10e3; % sampling rate [samp/s] // MAKE THIS A MULTIPLE OF 10!
signalBandwidth = 1e3; % signal bandwidth [Hz] (this sets the lowpass cutoff) // MAKE THIS A
SIMPLE FRACTION OF THE SAMPLING RATE!
nfftRaw = min(2^nextpow2(sampleRate/2), 2^15); % FFT size for raw PSD estimate
nfftBaseband = min(2^nextpow2(5*signalBandwidth), 2^15); % FFT size for baseband PSD
estimate
inputDuration = 0.1; % length of each input data read [s] (also sets plot update rate) // MAKE
THIS NO LESS THAN 0.1
windowDuration = 1.0; % length of plot window [s]
ampsPerVolt = 1e-6; % current preamplifier sensitivity [A/V]

% generate output signal
freqVin = 0.814e3; % frequency of sine excitation [Hz] // MAKE THIS NO MORE THAN 1/5th
OF THE SAMPLING RATE AND A MULTIPLE OF 10!
% freqVin = 0; % FOR DC ACQUISITION
Vpp = 1.0; % peak to peak voltage of excitation signal [V]
if freqVin == 0, Vpp = Vpp*2; end % amplitude fix for DC
outputDuration = 1; % length of each output data write [s] (1 second is fine)
outputData = Vpp/2 * cos(2*pi*freqVin*(0:outputDuration*sampleRate-1)/sampleRate).'; %
output data to write to output queue
demodSignal = 2 * exp(-1i*2*pi*freqVin*(0:inputDuration*sampleRate-1)/sampleRate).'; %
signal same length as the input data read for demodulation

% initialize PSD estimates
psdRaw = zeros(nfftRaw/2+1, 1);
psdBaseband = zeros(nfftBaseband/2+1, 1);

% fix resistance calculation...
if freqVin == 0, Vpp = Vpp*2; end
```

```
% initialize figure
figureHandle = figure; % open a new figure to plot in
set(figureHandle, 'Units', 'Normalized', 'OuterPosition', [0.1 0.1 0.9 0.9]); % almost fullscreen
subplot(3,1,1);
subplot(3,1,2);
subplot(3,1,3);
lineHandle = animatedline;

% set global variables so plotData callback function can access them
setGlobalPsdRaw(psdRaw);
setGlobalPsdBaseband(psdBaseband);
setGlobals(sampleRate, ...
        signalBandwidth, ...
        Vpp, ...
        ampsPerVolt, ...
        demodSignal, ...
        nfftRaw, ...
        nfftBaseband, ...
        inputDuration, ...
        windowDuration, ...
        lineHandle, ...
        figureHandle);

%% ACQUISITION INITIALIZATION
 % create and configure data acquisition session
s = daq.createSession('mcc');
addAnalogOutputChannel(s, 'Board0', 0, 'Voltage');
addAnalogInputChannel(s, 'Board0', [3,4,5], 'Voltage');

% set session parameters
s.Rate = sampleRate; % sampling rate [samp/s]
s.IsContinuous = true;
s.NotifyWhenDataAvailableExceeds = inputDuration * sampleRate; % this sets the input data
buffer read rate
s.NotifyWhenScansQueuedBelow = 5 * outputDuration * sampleRate; % this sets when to write
to the output queue

% open binary data log file
fid1 = fopen('log.bin', 'w');

% add callback function listeners
btn = uicontrol('Style', 'pushbutton', 'String', 'Stop', 'Position', [10 10 40 20], ...
            'Callback', 'stop(s); release(s)'); % this push button is supposed to stop the analog input
object
```

```
lh1 = addlistener(s, 'DataAvailable', @(src, event) plotDataMulti(src, event)); % plots data for every input data buffer read
lh2 = addlistener(s, 'DataAvailable', @(src, event) logDataMulti(src, event, fid1)); % logs data to file for every input data buffer read
lh3 = addlistener(s, 'DataRequired', @(src, event) src.queueOutputData(outputData)); % writes output data whenever output queue is low

%% START ACQUISITION
queueOutputData(s, repmat(outputData, round(10/outputDuration), 1)); % start with 10 seconds of output data
fprintf('Output samples in queue = %d\n', s.ScansQueued);
prepare(s);
pause(1); % just in case

s.startBackground(); % this starts the continuous acquisition
fprintf('Acquisition started!\n');
fprintf('Output samples in queue = %d\n', s.ScansQueued);

% loop for printouts
tic;
while s.IsRunning
   pause(5);
   fprintf('Elapsed time = %d seconds\n', round(toc));
   fprintf('Samples acquired = %d\n', s.ScansAcquired);
   fprintf('Output samples in queue = %d\n', s.ScansQueued);
end

% after completion, delete listeners
delete(lh1);
delete(lh2);
delete(lh3);
fclose(fid1);
fprintf('Acquisition stopped!\n');

%% load data into MATLAB from binary log
fid2 = fopen('log.bin', 'r');
[data, count] = fread(fid2, inf, 'double'); % load data into MATLAB
fclose(fid2);

return

%% save?

data = data.';
filename = input('Input file name: ', 's');
save([filename '.mat'], 'data', 'Vpp', '); % save the variables you want
```